Appl. Math. Mech. -Engl. Ed., **40**(4), 515–548 (2019)

Applied Mathematics and Mechanics (English Edition)

https://doi.org/10.1007/s10483-019-2482-9

Deep postbuckling and nonlinear bending behaviors of nanobeams with nonlocal and strain gradient effects*

Bo ZHANG[1,2,†], Huoming SHEN[1,2], Juan LIU[1,2],
Yuxing WANG[1,2], Yingrong ZHANG[1,2]

1. School of Mechanics and Engineering, Southwest Jiaotong University, Chengdu 611756, China;
2. Applied Mechanics and Structure Safety Key Laboratory of Sichuan Province, Chengdu 611756, China

(Received May 2, 2018 / Revised Aug. 12, 2018)

Abstract In this paper, multi-scale modeling for nanobeams with large deflection is conducted in the framework of the nonlocal strain gradient theory and the Euler-Bernoulli beam theory with exact bending curvature. The proposed size-dependent nonlinear beam model incorporates structure-foundation interaction along with two small scale parameters which describe the stiffness-softening and stiffness-hardening size effects of nanomaterials, respectively. By applying Hamilton's principle, the motion equation and the associated boundary condition are derived. A two-step perturbation method is introduced to handle the deep postbuckling and nonlinear bending problems of nanobeams analytically. Afterwards, the influence of geometrical, material, and elastic foundation parameters on the nonlinear mechanical behaviors of nanobeams is discussed. Numerical results show that the stability and precision of the perturbation solutions can be guaranteed, and the two types of size effects become increasingly important as the slenderness ratio increases. Moreover, the in-plane conditions and the high-order nonlinear terms appearing in the bending curvature expression play an important role in the nonlinear behaviors of nanobeams as the maximum deflection increases.

Key words nanobeam, nonlocal strain gradient theory, two-step perturbation method, deep postbuckling

Chinese Library Classification O344.1
2010 Mathematics Subject Classification 74H55

* Citation: ZHANG, B., SHEN, H. M., LIU, J., WANG, Y. X., and ZHANG, Y. R. Deep postbuckling and nonlinear bending behaviors of nanobeams with nonlocal and strain gradient effects. *Applied Mathematics and Mechanics* (*English Edition*), **40**(4), 515–548 (2019) https://doi.org/10.1007/s10483-019-2482-9

† Corresponding author, E-mail: zhbxnjt@163.com

Project supported by the National Natural Science Foundation of China (Nos. 11672252 and 11602204) and the Fundamental Research Funds for the Central Universities, Southwest Jiaotong University (No. 2682016CX096)

1 Introduction

Nanotechnology pioneered a new path for the synthesis and characterization of advanced multifunctional materials and inspired enormous attention in fundamental research and engineering application[1–2]. Nanomaterials with different compositions and geometric shapes have been discovered and fabricated during the past two decades and widely used as building blocks of micro/nano-electro-mechanical system (MEMS/NEMS) to accomplish adjustable performances[1,3–6]. Lots of experimental and numerical studies reported that nanostructures possess unique mechanical, chemical, electrical, and optical properties as compared with atom/molecule clusters and their bulk composites[7]. The further developments of MEMS/NEMS are directly correlated with a deep understanding of their mechanical properties. The correlation research indicated that there are two different mechanical characteristics exhibited in nanostructures, namely, stiffness-softening[8–11] and stiffness-hardening effects[12–17]. As an example, Treacy et al.[14] observed a trend for higher modulus with smaller tube diameters in the first measurement of Young's modulus of carbon nanotubes (CNTs). In contrast, Natsuki et al.[16] reported that Young's modulus of single-walled carbon nanotubes (SWCNTs) decreases with an increase in the tube diameter by using a universal force field for C-C bonds to study CNTs based on a structural mechanical approach. In the micro-bending test of epoxy polymeric micro-cantilevers, Lam et al.[12] found that the bending rigidity increases about 2.4 times as the beam thickness is reduced from 115 μm to 20 μm, while the deformation is still in the linear elastic region.

It is well known that the stress at a given material point in a body depends on the strain, strain rate, and strain history at that point in the classical continuum theory. It can be regarded as a scale-free continuum theory due to the absence of interatomic interactions among neighboring material points in the constitutive relation. Although classical continuum-based models are able to predict the mechanical behaviors of nanostructures to a certain extent[18–20], they are inadequate to capture the size effects accurately when the microscopic length scale is comparable with the macroscopic one. It is naturally believed that the interatomic spacing between individual atoms plays an increasingly important role at small scales, which leads that the discrete nature of nanostructures can no longer be homogenized into a continuum medium[1]. Taking size effects into consideration is therefore of prime importance for the reliable and optimal design of nanodevices. Several size-dependent continuum theories have been proposed to overcome the shortcomings of classical theory through tireless efforts and arduous exploration, among which are the nonlocal elasticity theory[21–22], the strain gradient theory[23–24], the couple stress theory[25–26], and their improved versions[12,27–29]. The following briefly introduces the background and basic idea of some typical nonclassical theories.

The nonlocal elasticity theory assumes that the stress at a reference point is a function of strains at all points in the continuum. Its systematic and rational framework was initiated by Eringen[21] in the study of long-range phenomena in extended atomic systems. The original nonlocal constitutive relations involve an integral with weighted average of the local stress contribution from all points in the body, and are often termed the strong or integral nonlocal model. Given the mathematical difficulties in solving integral-differential governing equations, Eringen[22] transformed the constitutive relations from an integral type to an approximate equivalent differential type and proved its feasibility. The practical importance and potential benefits of the differential nonlocal model have aroused continuing research interest until Peddieson et al.[30] applied it in the modeling of the static bending problem of CNTs based on the Euler-Bernoulli beam theory. Since then, a series of research work has sprung up in authoritative journals of applied mechanics in the past decade and a half. We limit ourselves to mention the works of Wang et al.[31], Lim and Wang[32], Hu et al.[33], Reddy[34], Shen and Zhang[35–36], Peng et al.[37], Ghorbanpour-Arani[38], and so on. Excellent overviews of various nonlocal continuum-based models and their applications in nanostructures can be found in

Ref. [1]. The corresponding results revealed the stiffness-softening size effect in nonlocal elastic models.

Although nonlocal continuum-based modeling of nanostructures has now reached a mature stage, it seems powerless to identify the mechanical characteristics with the stiffness-hardening size effect[12–13,15–17]. In view of this, some researchers suggested that introducing additional high-order strain gradient terms into the framework of classical continuum theory may resolve the above problem, which is the basic idea of the gradient elasticity theory. The gradient elasticity theory argues that the materials should be viewed as atoms with high-order deformation mechanism at small scale rather than just modelled as collections of points. In existing versions of the gradient theory, Yang's couple stress theory[28] and Lam's strain gradient elasticity theory[12] are the two most widely applied in the modeling and analysis of micro/nanostructures. The former introduces the strain tensor and the symmetric part of the rotation gradient tensor in the strain energy density function, while the latter is more extensive and applicable because it contains the symmetric part of rotation gradient tensor as well as the dilatation and deviatoric stretch gradient tensors. The two theories have attracted considerable attention in the filed of micro/nanomechanics in the past decade. A large number of linear or nonlinear size-dependent beam, plate, and shell continuum models have been proposed for investigating various mechanical problems of micro/nanostructures. This topic is covered extensively in the literature, but here we just mention the typical studies of Park and Gao[39], Ma et al.[40], Şmşk and Reddy[41], Reddy and Kim[42], Komijani et al.[43], Kong et al.[44], Wang et al.[45–46], Mohammadimehr et al.[47], and Zhang et al.[48], in which the stiffness-hardening phenomena can be observed.

The above-mentioned two types of continuum theories manifested that the nonlocal and the strain gradient continuum-based models characterize two entirely different size-dependent behaviors of small scale materials. To predict the effects of long-range force and high-order deformation mechanism of microstructure reasonably, it is necessary and urgent to bring both nonlocal and strain gradient length scale parameters into a unified framework. To this end, Lim et al.[2] successfully extended the theoretical framework of classical nonlocal theory by combining the nonlocality of high-order stress field into the stored energy function, and proposed a comprehensive theory named the nonlocal strain gradient theory. Accocrding to the generalized differential constitutive equation, Lim et al.[2] presented the Euler-Bernoulli and Timoshenko beam models and illustrated their application values by taking the wave propagation problem of CNTs as an example. After that, nonlocal strain gradient-based modeling and simulation have come into a stage of booming development. Li and his partner performed a series of work in applying the one-dimensional nonlocal strain gradient models to investigate the mechanical problems of nanostructures, including buckling and postbuckling[49–51], linear and nonlinear static bending[51–52], linear and nonlinear flexural vibration[51–53], and flexural wave propagation[54]. Sahmani and Fattahi[55] developed an axially loaded functionally graded nonlocal strain gradient nanoshell model and conducted buckling and postbuckling analysis by a two-stepped perturbation technique. Lu et al.[56–58] studied the size-dependent mechanical behaviors of Kirchhoff and Mindlin plates and higher-order shear deformable beams by using the nonlocal strain gradient theory and obtained Navier solutions for simply supported boundary conditions.

Micro/nanobeams are the core structures in MEMS/NEMS and are frequently used as nanosensors and nanoactuators for sensing and energy harvesting. Besides, nanostructures such as nanowires and CNTs are shaped like slender tubular structures with high length-to-diameter ratio, in which their motion and deformation behaviors can be simulated by an elastic beam under external loads. Many studies showed that the geometric nonlinearity, mainly coming from the nonlinear moment-curvature relationship and midplane stretching, cannot be neglected as the beams deflect at the order of its thickness and remain elastic and the linear beam theory will lose its validity. To describe the deformation and motion behaviors of beams more accurately, Shen[59] proposed an exact bending curvature model for the nonlinear analysis of macroscopic

beams with movable/immovable end conditions, and then solved three typical kinds of nonlinear mechanical problems by a two-step perturbation technique. Accordingly, Shen and Zhang[36] established a nonlocal beam model for large deflected SWCNTs in thermal environments. Li and Qiao[60] conducted geometrically nonlinear free vibration investigation of anisotropic laminated composite beams based on a Reddy's shear deformation theory with a von Kármán-type of kinematic nonlinearity and an exact bending curvature model. It is worth reminding that the relevant studies[36,59–60] used the same bending curvature expression for both kinds of end conditions, but actually this treatment way is unacceptable for the immovable end conditions.

The above literature review demonstrates that there are no published works concerning nonlinear bending and postbuckling of nonlocal strain gradient nanobeams with large deflection resting on an elastic foundation. The present work fills this gap in the literature by considering nanobeams with two types of in-plane boundary conditions, namely, movable and immovable. For the postbuckling problem, one end of the beam is assumed to be movable, and for the nonlinear bending problem, movable and immovable end conditions are considered. The nonlinear motion equation and related boundary conditions including the foundation-structure interaction are derived by using the variational principle. Using the two-step perturbation method, the nonlinear bending load-deflection curves and postbuckling equilibrium paths are obtained. Extensive parametric studies are performed to establish the convergence and accuracy of the perturbation solutions and to probe into the nonlinear bending and postbuckling behaviors.

2 Nonlocal strain gradient theory

In the framework of nonlocal strain gradient theory, the stored strain energy U_0 for isotropic linear elastic materials occupying the region Ω is expressed as[2]

$$\begin{aligned} U_0(x) =& \frac{1}{2}\varepsilon_{ij}(x)C_{ijkl}\int_\Omega \alpha_0(|x-\hat{x}|,\ e_0a)\varepsilon_{kl}(\hat{x})\mathrm{d}\Omega \\ &+ \frac{1}{2}l^2\varepsilon_{ij,m}(x)C_{ijkl}\int_\Omega \alpha_1(|x-\hat{x}|,\ e_1a)\varepsilon_{kl,m}(\hat{x})\mathrm{d}\Omega, \end{aligned} \tag{1}$$

where x and $\hat{x}$ are the field and source points, respectively, ε_{ij} and $\varepsilon_{ij,m}$ are the strain and strain gradient tensors, respectively, C_{ijkl} is the fourth-order elasticity tensor, e_0 and e_1 are the low- and high-order nonlocal parameters obtained from a comparison of the wave dispersion relation and the experimental data or atomic lattice dynamics, respectively, a is an internal characteristic length, α_0 and α_1 are the attenuation kernel functions describing the nonlocality of strain and strain gradient fields, respectively, l is a material length scale parameter indicating the significance of the strain gradient field, and a comma followed by a subscript denotes differentiation with respect to the subscript.

Using Eq. (1), the constitutive equations can be readily obtained,

$$\sigma_{ij}^{[\mathrm{l}]} = C_{ijkl}\int_\Omega \alpha_0(|x-\hat{x}|,\ e_0a)\varepsilon_{kl}(\hat{x})\mathrm{d}\Omega, \tag{2a}$$

$$\sigma_{ijm}^{[\mathrm{h}]} = l^2C_{ijkl}\int_\Omega \alpha_1(|x-\hat{x}|,\ e_1a)\varepsilon_{kl,m}(\hat{x})\mathrm{d}\Omega, \tag{2b}$$

in which $\sigma_{ij}^{[\mathrm{l}]}$ and $\sigma_{ijm}^{[\mathrm{h}]}$ are the low- and high-order nonlocal stress tensors, respectively. One can see that the two tensors at a specific point rely on the strain along with its gradient not only at that point, but also at all the other points of the body. The total stress tensor $\sigma_{ij}^{[\mathrm{t}]}$ is defined by

$$\sigma_{ij}^{[\mathrm{t}]} = \sigma_{ij}^{[\mathrm{l}]} - \sigma_{ijm,m}^{[\mathrm{h}]}. \tag{3}$$

Obviously, the nonlocal strain gradient theory can degenerate into the pure strain gradient theory without stress nonlocality by setting both e_0a and e_1a to be zero. The nonlocal

attenuation kernel functions should satisfy the following relations:

$$\lim_{e_0\to\infty}\alpha_0(|x-\hat{x}|,\ e_0a)=\delta(|x-\hat{x}|),\quad \lim_{e_1\to\infty}\alpha_1(|x-\hat{x}|,\ e_1a)=\delta(|x-\hat{x}|). \tag{4}$$

From Eqs. (2a) and (2b), it is obvious that the low-order and high-order nonlocal stress fields are expressed in the convolution form of strain and strain gradient fields, respectively, which will bring some difficulties into the continuum-based modeling and analytical/numerical-based solving. On account of this, Lim et al.[2] proposed a differential form of constitutive equation following a procedure stemmed from Eringen[22], that is

$$(1-(e_1a)^2\nabla^2)(1-(e_0a)^2\nabla^2)\sigma_{ij}^{[\mathrm{t}]}=C_{ijkl}(1-(e_1a)^2\nabla^2)\varepsilon_{kl}-l^2C_{ijkl}(1-(e_0a)^2\nabla^2)\nabla^2\varepsilon_{kl}, \tag{5}$$

in which ∇^2 is the Laplacian operator. Equation (5) realizes the combination of the classical nonlocal theory and the pure strain gradient theory, and can recover the constitutive equation of one of the two under certain conditions.

3 Description of geometric deformation of large deflected nanobeams

Figures 1(a) and 1(b) illustrate the schematic diagram of a simply supported nanobeam with movable and immovable end conditions, respectively, in which the Cartesian coordinate system with its origin coinciding with the midplane is introduced to describe the configuration. The symbols $\mathrm{d}X$ and $\mathrm{d}S$ denote the lengths of infinitesimal element before and after deformation, respectively. The X-, Y-, and Z-coordinate axes are taken along the length, width, and thickness directions, respectively. The capital L, A, J, E, P, and Q denote the length, cross-sectional area, inertia moment, elasticity modulus, constant axial force applied to the two ends, and transverse force distributed along the X-axis, respectively. The elastic foundation is assumed to be an adhering Pasternak-type in line with routine, which means that the nanobeam always keeps contact with the elastic foundation before and after large deflection. The relationship between the additional load and the displacement of foundation is described by $P_{\mathrm{ef}}=K_1W-K_2\frac{\partial^2W}{\partial X^2}$, where P_{ef} is the force per unit area, and K_1 and K_2 are the Winkler and Pasternak stiffnesses, respectively[59]. The nanobeam is modeled based on the nonlocal strain gradient theory and Kirchhoff's deformation hypothesis, which supposes that the straight line perpendicular to the midplane initially remains straight line perpendicular to the midplane henceforth. For the beams with large deflection, one needs to pay special attention to the adopted physical assumption and the truncation order of exact bending curvature expression. In other words,

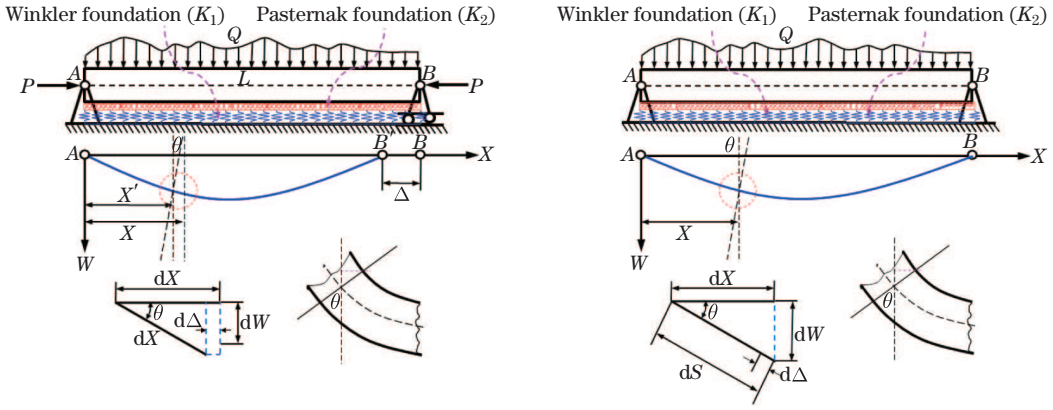

(a) Movable end (b) Immovable end

Fig. 1 Coordinate system and deformation kinematics of simply supported nanobeam resting on two-parameter elastic foundation

the sufficient high-order nonlinear terms are needed to examine the moderate rotational range of beam deformation as the truncation order strongly affects the results. For buckling analysis, at least one end of the beam should be movable, or else the physically incorrect results will be led to, as pointed out by Shen[59] and Li and Qiao[60].

For a nanobeam with a freely movable end condition, the nonlinear moment-curvature relationship becomes prominent as the inextensibility condition is considered. The length of line element $\mathrm{d}X$ in the neutral axis keeps unchanged before and after deformation, i.e.,

$$(\mathrm{d}X)^2 = (\mathrm{d}X - \mathrm{d}\Delta)^2 + (\mathrm{d}W)^2, \tag{6}$$

where $\mathrm{d}\Delta$ and $\mathrm{d}W$ are, respectively, the infinitesimal horizontal and vertical displacements of the material point $(X + \mathrm{d}X, 0, 0)$ with respect to its neighbouring point $(X, 0, 0)$. According to Fig. 1(a), the horizontal displacement of a material point located at $(X, 0, 0)$ is

$$\Delta = -\int_0^X \Big(1 - \sqrt{1 - \Big(\frac{\partial W}{\partial \widehat{X}}\Big)^2}\Big)\mathrm{d}\widehat{X}. \tag{7}$$

The cross-section rotation angle θ relative to the Y-axis and the midplane bending curvature κ are

$$\theta = \arcsin\Big(\frac{\partial W}{\partial X}\Big), \tag{8}$$

$$\kappa = \frac{\partial \theta}{\partial X} = \frac{\partial^2 W}{\partial X^2}\Big/\sqrt{1 - \Big(\frac{\partial W}{\partial X}\Big)^2}. \tag{9}$$

In view of Eqs. (7)–(9) and recalling Kirchhoff's assumption, the horizontal and transverse displacements U_X and U_Z at any off-midplane point $(X, 0, Z)$ are presented in the following forms:

$$U_X = -\int_0^X \Big(1 - \sqrt{1 - \Big(\frac{\partial W}{\partial \xi}\Big)^2}\Big)\mathrm{d}\xi - Z\frac{\partial W}{\partial X}, \quad U_Y = 0, \quad U_Z = W - Z\Big(1 - \sqrt{1 - \Big(\frac{\partial W}{\partial X}\Big)^2}\Big). \tag{10}$$

For a nanobeam with a fully immovable end condition, the midplane stretching may occur. The length of line element $\mathrm{d}X$ in the neutral axis before deformation and that after deformation need to meet the following relationship:

$$(\mathrm{d}X + \mathrm{d}\Delta)^2 = (\mathrm{d}X)^2 + (\mathrm{d}W)^2, \tag{11}$$

in which $\mathrm{d}\Delta$ and $\mathrm{d}W$ are, respectively, the infinitesimal elongation of line element and the vertical displacement of the material point $(X + \mathrm{d}X,\ 0,\ 0)$ with respect to its neighbouring point $(X,\ 0,\ 0)$.

In this case, the cross-section rotation angle and the midplane bending curvature are

$$\theta = \arctan\Big(\frac{\partial W}{\partial X}\Big), \tag{12}$$

$$\kappa = \frac{\partial \theta}{\partial X} = \frac{\partial^2 W}{\partial X^2}\Big/\Big(1 + \Big(\frac{\partial W}{\partial X}\Big)^2\Big). \tag{13}$$

Comparing Eqs. (12) and (13) with Eqs. (8) and (9), we can see that the movable end condition and immovable one lead to different forms of the expressions of cross-section rotation angle and midplane bending curvature. However, the previous literature[36,59–60] adopted the same bending curvature expression for both movable and immovable nanobeams.

Taking into account Eqs. (12) and (13), the displacement field for the immovable end condition is given as

$$\begin{cases} U_X = -Z\dfrac{\partial W}{\partial X}\Big/\sqrt{1+\Big(\dfrac{\partial W}{\partial X}\Big)^2} \approx -Z\dfrac{\partial W}{\partial X}\Big(1-\dfrac{1}{2}\Big(\dfrac{\partial W}{\partial X}\Big)^2\Big), \quad U_Y = 0, \\ U_Z = W - Z\Big(1-1\Big/\sqrt{1+\Big(\dfrac{\partial W}{\partial X}\Big)^2}\Big) \approx W - \dfrac{1}{2}Z\Big(\dfrac{\partial W}{\partial X}\Big)^2, \end{cases} \tag{14}$$

in which the maximum deflection needs to be limited to a relatively small range since the necking phenomenon appearing in the deformation process cannot be neglected when the deflection has a relatively large value.

4 Nonlinear governing equations for size-dependent nanobeams

4.1 Movable end condition

To make the subsequent derived formulae more compact, different orders of partial derivatives of deflection with respect to the coordinate X or time t are abbreviated as

$$\frac{\partial^i W}{\partial X^i} = W_i, \quad \frac{\partial W}{\partial t} = W_t, \quad \frac{\partial^2 W}{\partial t^2} = W_{tt}. \tag{15}$$

Using Eq. (10), the nonzero component of the Green strain tensor is obtained as

$$\varepsilon_{XX} = \sqrt{\Big(1+\frac{\partial U_X}{\partial X}\Big)^2 + \Big(\frac{\partial U_Z}{\partial X}\Big)^2} - 1 = -\frac{ZW_2}{\sqrt{1-W_1^2}}, \tag{16}$$

from which it is obvious that the movable model has no midplane stretching effect.

Based on Eq. (16), the first- and second-order strain gradients can be obtained as

$$\varepsilon_{XXX} = \frac{\partial \varepsilon_{XX}}{\partial X} = -\frac{Z}{\sqrt{1-W_1^2}}\Big(W_3 + \frac{W_2^2 W_1}{1-W_1^2}\Big), \tag{17a}$$

$$\varepsilon_{XXXX} = \frac{\partial^2 \varepsilon_{XX}}{\partial X^2} = -\frac{Z}{\sqrt{1-W_1^2}}\Big(W_4 + \frac{3W_1W_2W_3 + W_2^3}{1-W_1^2} + \frac{3W_1^2W_2^3}{(1-W_1^2)^2}\Big). \tag{17b}$$

For the beam-like structure, its size-dependent behavior in both the width and thickness directions can be neglected[2]. Equation (5) degenerates to the following one-dimensional nonlocal strain gradient constitutive relation:

$$(1-(e_1a)^2\nabla^2)(1-(e_0a)^2\nabla^2)\sigma_{XX}^{[t]} = E(1-(e_1a)^2\nabla^2)\varepsilon_{XX} - El^2(1-(e_0a)^2\nabla^2)\nabla^2\varepsilon_{XX}. \tag{18}$$

In accordance with the assumption adopted by Lim et al.[2], i.e., retaining terms up to the order of $O(\nabla^2)$ and forcing $e_0a = e_1a = \eta$, Eq. (18) is simplified as

$$\sigma_{XX}^{[t]} - \eta^2\frac{\partial^2\sigma_{XX}^{[t]}}{\partial X^2} = E\Big(\varepsilon_{XX} - l^2\frac{\partial^2\varepsilon_{XX}}{\partial X^2}\Big). \tag{19}$$

Integrating Eq. (19) through the cross-section, the nonlocal force-deflection and moment-deflection are as follows:

$$N_{\rm c} - \eta^2\frac{\partial^2 N_{\rm c}}{\partial X^2} = EA\varphi(X), \tag{20a}$$

$$M_{\rm c} - \eta^2\frac{\partial^2 M_{\rm c}}{\partial X^2} = EJ\phi(X), \tag{20b}$$

in which

$$N_{\rm c}=\int_A \sigma_{XX}^{[{\rm t}]}{\rm d}A,\quad M_{\rm c}=\int_A Z\sigma_{XX}^{[{\rm t}]}{\rm d}A, \tag{21}$$

$$\varphi(X)=0,\quad \phi(X)=\frac{1}{\sqrt{1-W_1^2}}\Big(l^2\Big(W_4+3\frac{W_3W_1W_2}{1-W_1^2}+3\frac{W_2^3W_1^2}{(1-W_1^2)^2}+\frac{W_2^3}{1-W_1^2}\Big)-W_2\Big). \tag{22}$$

Equations (20a) and (20b) are the second-order differential equations. Their explicit solutions are obtained by the asymptotic expansion method employed by Lim and Wang[32], i.e.,

$$N_{\rm c}=\sum_{n=0}^{\infty}a_n\frac{{\rm d}^{2n}\varphi}{{\rm d}X^{2n}}=a_0\varphi+a_1\frac{{\rm d}^2\varphi}{{\rm d}X^2}+a_2\frac{{\rm d}^4\varphi}{{\rm d}X^4}+\cdots, \tag{23a}$$

$$M_{\rm c}=\sum_{n=0}^{\infty}b_n\frac{{\rm d}^{2n}\phi}{{\rm d}X^{2n}}=b_0\phi+b_1\frac{{\rm d}^2\phi}{{\rm d}X^2}+b_2\frac{{\rm d}^4\phi}{{\rm d}X^4}+\cdots, \tag{23b}$$

where $a_n=EA\eta^{2n}$, and $b_n=EJ\eta^{2n}$. For simplicity, the asymptotic solutions to Eqs. (23a) and (23b) are taken up to the second-order terms, i.e., $O({\rm d}^2\varphi/{\rm d}X^2)$.

The motion equation and related boundary conditions are derived by Hamilton's principle. The dynamic form of this principle is stated as

$$\delta\int_{t_1}^{t_1}(K_0-(U_0+U_{\rm ad}-W_{\rm e})){\rm d}t=0, \tag{24}$$

where U_0 is the strain energy, $W_{\rm e}$ is the work done by the external loads, K_0 is the kinetic energy, and $U_{\rm ad}$ is the additional strain energy induced by elastic foundation.

The first variation of the strain energy is given by

$$\begin{aligned}\delta U_0&=\int_V(\sigma_{XX}^{[{\rm l}]}\delta\varepsilon_{XX}+\sigma_{XX}^{[{\rm h}]}\nabla\delta\varepsilon_{XX}){\rm d}V\\&=\int_V\sigma_{XX}^{[{\rm t}]}\delta\varepsilon_{XX}{\rm d}V+\Big(\int_A\sigma_{XX}^{[{\rm h}]}\delta\varepsilon_{XX}{\rm d}A\Big)_{X=0}^{X=L}\\&=\int_0^L(\widehat{N}_{\rm c}\delta W_1-\widehat{M}_{\rm c}\delta W_2){\rm d}X+(\widehat{N}_{nc}\delta W_1-\widehat{M}_{\rm nc}\delta W_2)_{X=0}^{X=L}\\&=(\widehat{N}_{\rm c}\delta W)_{X=0}^{X=L}-\Big(\widehat{M}_{\rm c}\delta W_1-\frac{\partial\widehat{M}_{\rm c}}{\partial X}\delta W\Big)_{X=0}^{X=L}+(\widehat{N}_{nc}\delta W_1-\widehat{M}_{nc}\delta W_2)_{X=0}^{X=L}\\&\quad-\int_0^L\Big(\frac{\partial\widehat{N}_{\rm c}}{\partial X}+\frac{\partial^2\widehat{M}_{\rm c}}{\partial X^2}\Big)\delta W{\rm d}X,\end{aligned} \tag{25}$$

in which

$$\widehat{N}_{\rm c}=\frac{N_{\rm c}W_1}{\sqrt{1-W_1^2}}-\frac{M_{\rm c}W_2W_1}{(1-W_1^2)^{3/2}},\quad \widehat{M}_{\rm c}=\frac{M_{\rm c}}{\sqrt{1-W_1^2}}, \tag{26a}$$

$$\widehat{N}_{nc}=\frac{N_{nc}W_1}{\sqrt{1-W_1^2}}-\frac{M_{nc}W_2W_1}{(1-W_1^2)^{3/2}},\quad \widehat{M}_{nc}=\frac{M_{nc}}{\sqrt{1-W_1^2}}, \tag{26b}$$

where

$$N_{nc}=\int_A\sigma_{XX}^{[{\rm h}]}{\rm d}A,\quad M_{nc}=\int_A Z\sigma_{XX}^{[{\rm h}]}{\rm d}A. \tag{27}$$

The external work done by the applied loads and its first variation are expressed as

$$W_{\rm e}=\int_0^L(QW+P(1-\sqrt{1-W_1^2})){\rm d}X,\quad \delta W_{\rm e}=\int_0^L\Big(Q-\frac{\partial\widehat{P}}{\partial X}\Big)\delta W{\rm d}X+(\widehat{P}\delta W)_{x=0}^{x=L}, \tag{28}$$

in which $\widehat{P} = PW_1/\sqrt{1-W_1^2}$.

The first variation of the deformation energy of elastic foundation can be written as

$$\delta U_{\rm ad} = \int_0^L (K_1 W - K_2 W_2)\delta W \mathrm{d}X + (K_2 W_1 \delta W)_{X=0}^{X=L}. \tag{29}$$

Substituting Eqs. (25), (27), (28), and (29) into Eq. (24), integrating by parts, and then setting the coefficient of δW to zero, the following equation of motion can be obtained:

$$\frac{\partial \widehat{N}_{\rm c}}{\partial X} + \frac{\partial^2 \widehat{M}_{\rm c}}{\partial X^2} - K_1 W + K_2 W_2 + Q - \frac{\partial \widehat{P}}{\partial X} = 0 \tag{30}$$

together with the boundary conditions

$$W = 0 \quad \text{or} \quad \widehat{N}_{\rm c} + \frac{\partial \widehat{M}_{\rm c}}{\partial X} + K_2 W_1 - \widehat{P} = 0, \tag{31a}$$

$$W_1 = 0 \quad \text{or} \quad \widehat{M}_{\rm c} - \widehat{N}_{nc} = 0, \tag{31b}$$

$$W_2 = 0 \quad \text{or} \quad \widehat{M}_{nc} = 0. \tag{31c}$$

Substituting the second-order asymptotic solutions of Eqs. (23a) and (23b) into Eq. (30) yields the motion equation in terms of the deflection, i.e.,

$$-PW_2\Lambda(1+\Lambda^2 W_1^2) + Q + K_2 W_2 - K_1 W_0 + EJ\sum_0^{14} a_{EJ}^{(i)}\Lambda^i = 0, \tag{32}$$

in which

$$\begin{cases}
\Lambda = 1/\sqrt{1-W_1^2}, \quad a_{EJ}^{(1)} = a_{EJ}^{(3)} = a_{EJ}^{(5)} = a_{EJ}^{(7)} = a_{EJ}^{(9)} = a_{EJ}^{(11)} = a_{EJ}^{(13)} = 0, \\
a_{EJ}^{(2)} = \eta^2 l^2 W_8 + W_6(l^2-\eta^2) - W_4, \\
a_{EJ}^{(4)} = (21W_3(W_1W_6 + 5W_2W_5) + 35W_4(W_1W_5 + 3W_3^2) \\
\qquad + W_2(21W_2W_6 + 70W_4^2 + 8W_1W_7))l^2\eta^2 + (10W_4(W_2^2 + W_1W_3) \\
\qquad + 3W_2(5W_3^2 + 2W_1W_5))(l^2-\eta^2) - W_2(4W_1W_3 + W_2^2), \\
a_{EJ}^{(6)} = (315(W_2^4W_4 + W_1^2W_3^2W_4 + 3W_2^3W_3^2) + 110W_1W_2(3W_2^2W_5 \\
\qquad + 3W_1W_5W_3 + 2W_1W_4^2) + 3W_1W_2(320W_3^3 + 23W_1W_2W_6 + 650W_2W_4W_3))l^2\eta^2 \\
\qquad - 4W_1^2W_2^3 + (48W_1W_2W_3(2W_2^2 + W_1W_3) + W_2^2(9W_2^3 + 34W_1^2W_4))(l^2-\eta^2), \\
a_{EJ}^{(8)} = (1\ 620W_1W_2W_3(W_1^2W_3^2 + 3W_2^4) + 30W_1^2W_2^2(19W_1W_2W_5 \\
\qquad + 111W_2^2W_4 + 111W_1W_3W_4) + 45W_2^3(5W_2^4 + 219W_1^2W_3^2))l^2\eta^2 \\
\qquad + 3W_1^2W_2^3(33W_2^2 + 56W_1W_3)(l^2-\eta^2), \\
a_{EJ}^{(10)} = 75(W_1^2W_2^4(66W_2^3 + 53W_1^2W_4) + 156W_1^3W_2^3W_3(2W_2^2 + W_1W_3))l^2\eta^2 \\
\qquad + 120W_1^4W_2^5(l^2-\eta^2), \\
a_{EJ}^{(12)} = 105W_1^4W_2^5(145W_2^2 + 204W_1W_3)l^2\eta^2, \quad a_{EJ}^{(14)} = 11\ 340W_1^6W_2^7\eta^2l^2.
\end{cases} \tag{33}$$

Setting $l = \eta = 0$, Eq. (32) reduces to the following form:

$$\frac{EJW_4}{1-W_1^2} + \frac{4EJW_1W_2W_3}{(1-W_1^2)^2} + \frac{EJW_2^3(1+3W_1^2)}{(1-W_1^2)^3} + \frac{PW_2}{(1-W_1^2)^{3/2}} - Q - K_2W_2 + K_1W_0 = 0, \tag{34}$$

which is the motion equation of classical exact bending curvature beam model developed by Shen[59].

Conducting the Taylor expansion for $\Lambda=1/\sqrt{1-W_1^2}$ with respect to W_1 around the origin, retaining the first four order terms, i.e., $\Lambda \approx 1+W_1^2/2+3W_1^4/8+5W_1^6/16$, and then substituting it into Eq. (32), we can obtain

$$\begin{aligned}
&-\frac{1}{16}PW_2(24W_1^2+30W_1^4+35W_1^6+16)+Q+K_2W_2-K_1W_0-\rho AW_{tt}\\
&+EJ(A_{EJ}^{(8)}W_8+A_{EJ}^{(7)}W_7+A_{EJ}^{(6)}W_6+A_{EJ}^{(5)}W_5+A_{EJ}^{(42)}W_4^2+A_{EJ}^{(41)}W_4\\
&+A_{EJ}^{(33)}W_3^3+A_{EJ}^{(32)}W_3^2+A_{EJ}^{(31)}W_3+A_{EJ}^{(27)}W_2^7+A_{EJ}^{(25)}W_2^5+A_{EJ}^{(23)}W_2^3)=0, \qquad (35)
\end{aligned}$$

where

$$\begin{cases}
A_{EJ}^{(8)}=(W_1^6+W_1^4+W_1^2+1)\eta^2l^2, \quad A_{EJ}^{(7)}=8W_1W_2(1+2W_1^2+3W_1^4+4W_1^6)l^2\eta^2,\\
A_{EJ}^{(6)}=3((37+90W_1^2+166W_1^4)W_1^2W_2^2+7(4W_1^6+3W_1^4+2W_1^2+1)W_1W_3\\
\qquad +7W_2^2)l^2\eta^2+(W_1^6+W_1^4+W_1^2+1)(l^2-\eta^2),\\
A_{EJ}^{(5)}=5(3(160W_1^6+87W_1^4+36W_1^2+7)W_2W_3+6(11+52W_1^2+142W_1^4\\
\qquad +300W_1^6)W_1W_2^3+7(4W_1^6+3W_1^4+2W_1^2+35)W_1W_4)l^2\eta^2\\
\qquad +6W_1W_2(1+2W_1^2+3W_1^4+4W_1^6)(l^2-\eta^2),\\
A_{EJ}^{(42)}=10W_2(160W_1^6+87W_1^4+36W_1^2+7)l^2\eta^2,\\
A_{EJ}^{(41)}=15(2(65+306W_1^2+834W_1^4+1\ 760W_1^6)W_1W_2^2W_3+(21+285W_1^2\\
\qquad +1\ 279W_1^4+3\ 755W_1^6)W_2^4+7(1+5W_1^2+12W_1^4+22W_1^6)W_3^2)l^2\eta^2\\
\qquad +(2(5+27W_1^2+66W_1^4+122W_1^6)W_2^2+10(1+2W_1^2+3W_1^4+4W_1^6)W_1W_3)\\
\qquad \cdot(l^2-\eta^2)-(1+W_1^2+W_1^4+W_1^6),\\
A_{EJ}^{(33)}=60W_1W_2(16+75W_1^2+204W_1^4+430W_1^6)l^2\eta^2,\\
A_{EJ}^{(32)}=3W_2(15W_2^2(282W_1^2+1\ 262W_1^4+3\ 700W_1^6+21)l^2\eta^2\\
\qquad +(5+26W_1^2+63W_1^4+116W_1^6)(l^2-\eta^2)),\\
A_{EJ}^{(31)}=180W_1W_2^5(3\ 204W_1^6+1\ 039W_1^4+238W_1^2+27)l^2\eta^2\\
\qquad +24W_1W_2^3(110W_1^6+52W_1^4+19W_1^2+4)l^2\\
\qquad -24W_1W_2^3(110W_1^6+52W_1^4+19W_1^2+4)\eta^2\\
\qquad -4W_1W_2(4W_1^6+3W_1^4+2W_1^2+1),\\
A_{EJ}^{(27)}=(181\ 440W_1^6+42\ 225W_1^4+5\ 850W_1^2+225)l^2\eta^2,\\
A_{EJ}^{(25)}=(1\ 680W_1^6+570W_1^4+126W_1^2+9)(l^2-\eta^2),\\
A_{EJ}^{(23)}=-(4W_1^2+1)(7W_1^4+2W_1^2+1).
\end{cases} \qquad (36)$$

It is noticeable that the asymptotic expansion form of the classical exact bending curvature beam model developed in the literature[59] can be readily recovered by setting $l=\eta=0$, i.e.,

$$\begin{aligned}
&-\frac{1}{16}PW_2(24W_1^2+30W_1^4+35W_1^6+16)-EJ(4W_1W_2(1+2W_1^2+3W_1^4+4W_1^6)W_3\\
&+(1+W_1^2+W_1^4+W_1^6)W_4+(28W_1^6+15W_1^4+6W_1^2+1)W_2^3)+Q+K_2W_2-K_1W_0=0. \qquad (37)
\end{aligned}$$

Before carrying out the solution process, the following dimensionless quantities are intro-

duced:

$$\begin{cases} x=\dfrac{\pi X}{L}, \quad w=\dfrac{W}{L}, \quad \dfrac{\partial^i w}{\partial x^i}=w_i, \quad \dfrac{\partial W}{\partial X}=\pi w_1, \quad \dfrac{\partial^i W}{\partial X^i}=\dfrac{\pi^i w_i}{L^{i-1}}, \quad k_1=\dfrac{K_1 L^4}{\pi^4 EJ}, \\ k_2=\dfrac{K_2 L^2}{\pi^2 EJ}, \quad \lambda_p=\dfrac{PL^2}{\pi^2 EJ}, \quad \lambda_q=\dfrac{QL^3}{\pi^4 EJ}, \\ d_1=\dfrac{A\eta^2 l^2}{JL^2}, \quad d_2=\dfrac{A(l^2-\eta^2)}{J}, \quad d_3=\dfrac{AL^2}{\pi^2 J}, \quad d_4=\dfrac{\eta^2 l^2}{L^4}, \quad d_5=\dfrac{l^2-\eta^2}{L^2}. \end{cases} \tag{38}$$

Using the above dimensionless quantities, Eq. (35) can be rewritten as

$$\begin{aligned} &-\frac{1}{16}\lambda_p w_2(16+24\pi^2 w_1^2+30 w_1^4\pi^4+35\pi^6 w_1^6)+\lambda_q+k_2 w_2-k_1 w_0+\overline{A}_{EJ}^{(8)} w_8 \\ &+\overline{A}_{EJ}^{(7)} w_7+\overline{A}_{EJ}^{(6)} w_6+\overline{A}_{EJ}^{(5)} w_5+\overline{A}_{EJ}^{(42)} w_4^2+\overline{A}_{EJ}^{(41)} w_4+\overline{A}_{EJ}^{(33)} w_3^3+\overline{A}_{EJ}^{(32)} w_3^2 \\ &+\overline{A}_{EJ}^{(31)} w_3+\overline{A}_{EJ}^{(27)} w_2^7+\overline{A}_{EJ}^{(25)} w_2^5+\overline{A}_{EJ}^{(23)} w_2^3=0, \end{aligned} \tag{39}$$

in which

$$\begin{cases} \overline{A}_{EJ}^{(8)}=d_4\pi^4(\pi^6 w_1^6+\pi^2 w_1^2+\pi^4 w_1^4+1), \\ \overline{A}_{EJ}^{(7)}=8d_4\pi^6 w_1 w_2(1+4\pi^6 w_1^6+3\pi^4 w_1^4+2\pi^2 w_1^2), \\ \overline{A}_{EJ}^{(6)}=3d_4\pi^6(7w_1 w_3(1+2\pi^2 w_1^2+3\pi^4 w_1^4+4\pi^6 w_1^6)+w_2^2(166\pi^6 w_1^6+90\pi^4 w_1^4 \\ \qquad +37\pi^2 w_1^2+7))+d_5\pi^2(\pi^6 w_1^6+\pi^2 w_1^2+\pi^4 w_1^4+1), \\ \overline{A}_{EJ}^{(5)}=5d_4\pi^6(3(160\pi^6 w_1^6+87\pi^4 w_1^4+36\pi^2 w_1^2+7)w_2 w_3+7w_1 w_4(1+2\pi^2 w_1^2 \\ \qquad +3\pi^4 w_1^4+4\pi^6 w_1^6)+6\pi^2 w_1 w_2^3(300\pi^6 w_1^6+142\pi^4 w_1^4+52\pi^2 w_1^2+11)) \\ \qquad +6d_5\pi^4 w_1 w_2(1+4\pi^6 w_1^6+3\pi^4 w_1^4+2\pi^2 w_1^2), \\ \overline{A}_{EJ}^{(42)}=10d_4\pi^6 w_2(87\pi^4 w_1^4+160\pi^6 w_1^6+36\pi^2 w_1^2+7), \\ \overline{A}_{EJ}^{(41)}=15d_4\pi^6(\pi^2 w_2^4(21+285\pi^2 w_1^2+1\ 279\pi^4 w_1^4+3\ 755\pi^6 w_1^6) \\ \qquad +2\pi^2 w_1 w_2^2 w_3(306\pi^2 w_1^2+65+834\pi^4 w_1^4+1\ 760\pi^6 w_1^6)+7w_3^2(1+5\pi^2 w_1^2 \\ \qquad +12\pi^4 w_1^4+22\pi^6 w_1^6))+2d_5\pi^4(w_2^2(5+27\pi^2 w_1^2+66\pi^4 w_1^4+122\pi^6 w_1^6) \\ \qquad +5w_1 w_3(1+2\pi^2 w_1^2+3\pi^4 w_1^4+4\pi^6 w_1^6))-(\pi^6 w_1^6+\pi^2 w_1^2+\pi^4 w_1^4+1), \\ \overline{A}_{EJ}^{(33)}=60d_4\pi^8 w_1 w_2(430\pi^6 w_1^6+204\pi^4 w_1^4+16+75\pi^2 w_1^2), \\ \overline{A}_{EJ}^{(32)}=45d_4\pi^8 w_2^3(21+3\ 700\pi^6 w_1^6+1\ 262\pi^4 w_1^4+282\pi^2 w_1^2) \\ \qquad +3d_5\pi^4 w_2(5+116\pi^6 w_1^6+63\pi^4 w_1^4+26\pi^2 w_1^2), \\ \overline{A}_{EJ}^{(31)}=180d_4\pi^{10} w_1 w_2^5(27+1\ 039\pi^4 w_1^4+238\pi^2 w_1^2+3\ 204\pi^6 w_1^6) \\ \qquad +24d_5\pi^6 w_1 w_2^3(4+19\pi^2 w_1^2+110\pi^6 w_1^6+52\pi^4 w_1^4) \\ \qquad -4\pi^2 w_1 w_2(1+4\pi^6 w_1^6+3\pi^4 w_1^4+2\pi^2 w_1^2), \\ \overline{A}_{EJ}^{(27)}=15\,d_4\pi^{10}(390\,\pi^2 w_1^2+2\ 815\,\pi^4 w_1^4+12\ 096\,\pi^6 w_1^6+15), \\ \overline{A}_{EJ}^{(25)}=3\,d_5\pi^6(3+560\,\pi^6 w_1^6+190\,\pi^4 w_1^4+42\,\pi^2 w_1^2), \\ \overline{A}_{EJ}^{(23)}=-\pi^2(28\,\pi^6 w_1^6+15\,\pi^4 w_1^4+6\,\pi^2 w_1^2+1). \end{cases} \tag{40}$$

4.2 Immovable end condition

For a nanobeam with a fully immovable end condition, the axial compressive load cannot be applied. From Eq. (14), the expression of geometrically nonlinear strain is obtained as

$$\varepsilon_{XX}=\sqrt{\Big(1+\frac{\partial U_X}{\partial X}\Big)^2+\Big(\frac{\partial U_Z}{\partial X}\Big)^2}-1\approx\frac{1}{2}W_1^2-ZW_2, \tag{41}$$

where ZW_2 and $W_1^2/2$ denote the pure bending and midplane stretching deformation, respectively. It should be pointed out that the hypothesis of Wickert[61] is widely used in the nonlinear analysis of beam structures with the immovable end condition. Thereinto, the midplane stretching is viewed as a result of imposing on an approximate but equivalent axial force to prevent the edges motion[60]. This indicates that the midplane stretching and bending components of deformation are independent of each other.

Under Wickert's hypothesis[61], the pure axial tensile strain $\varepsilon_{XX}^{[\mathrm{s}]}$ is expressed by the volume averaging of geometrically nonlinear strain, i.e.,

$$\varepsilon_{XX}^{[\mathrm{s}]}=\frac{1}{\Omega}\int_\Omega\varepsilon_{XX}\mathrm{d}\Omega=\frac{1}{2L}\int_0^L W_1^2\mathrm{d}X, \tag{42}$$

where $\Omega=AL$ is the occupied space of the elastic beam.

The axial force induced by the midplane stretching is given by

$$N_0=EA\varepsilon_{XX}^{[\mathrm{s}]}=\frac{EA}{2L}\int_0^L W_1^2\mathrm{d}X. \tag{43}$$

The pure bending strain $\varepsilon_{XX}^{[\mathrm{b}]}$ induced by the cross-section moderate rotation is

$$\varepsilon_{XX}^{[\mathrm{b}]}=-ZW_2. \tag{44}$$

Obviously, the pure stretching strain no longer generates the strain gradient in the current circumstance, and the gradient of axial force N_0 equals zero. Therefore, the strain gradient is only sourced from the pure bending strain. Applying Eq. (44), the first- and second-order strain gradients are given as

$$\varepsilon_{XXX}^{[\mathrm{b}]}=\frac{\partial\varepsilon_{XX}^{[\mathrm{b}]}}{\partial X}=-ZW_3,\quad \varepsilon_{XXXX}^{[\mathrm{b}]}=\frac{\partial^2\varepsilon_{XX}^{[\mathrm{b}]}}{\partial X^2}=-ZW_4. \tag{45}$$

Equation (19) should be improved as the following form in terms of pure bending strain gradient $\varepsilon_{XX}^{[\mathrm{b}]}$ and its corresponding stress gradient $\sigma_{XX}^{[t_\mathrm{b}]}$, i.e.,

$$\sigma_{XX}^{[t_\mathrm{b}]}-\eta^2\frac{\partial^2\sigma_{XX}^{[t_\mathrm{b}]}}{\partial X^2}=E\Big(\varepsilon_{XX}^{[\mathrm{b}]}-l^2\frac{\partial^2\varepsilon_{XX}^{[\mathrm{b}]}}{\partial X^2}\Big). \tag{46}$$

The nonlocal axial force-deflection and bending moment-deflection relationships can be calculated by integrating Eq. (46) through the cross-section area, i.e.,

$$N_\mathrm{c}^{[t_\mathrm{b}]}-\eta^2\frac{\partial^2N_\mathrm{c}^{[t_\mathrm{b}]}}{\partial X^2}=EA\varphi(X),\quad M_\mathrm{c}^{[t_\mathrm{b}]}-\eta^2\frac{\partial^2M_\mathrm{c}^{[t_\mathrm{b}]}}{\partial X^2}=EJ\phi(X), \tag{47}$$

in which

$$\varphi(X)=0,\quad \phi(X)=l^2W_4. \tag{48}$$

The solutions to Eq. (47) can be asymptotically expressed in terms of φ and ϕ with the similar forms as Eqs. (23a) and (23b) and are truncated up to second-order terms.

The first variation of the strain energy of immovable nanobeam is given by

$$\begin{aligned}\delta U_0 &= \int_V (\sigma_{XX}^{[\mathrm{l}]}\delta\varepsilon_{XX} + \sigma_{XX}^{[\mathrm{h}]}\nabla\delta\varepsilon_{XX})\mathrm{d}V \\ &= \int_V \sigma_{XX}^{[\mathrm{t}]}\delta\varepsilon_{XX}\mathrm{d}V + \Big(\int_A \sigma_{XX}^{[\mathrm{h}]}\delta\varepsilon_{XX}\mathrm{d}A\Big)_{X=0}^{X=L} \\ &= \int_0^L (\widehat{N}_{\mathrm{c}}\delta W_1 - \widehat{M}_{\mathrm{c}}\delta W_2)\mathrm{d}X + ((\widehat{N}_{nc}\delta W_1 - \widehat{M}_{nc}\delta W_2))_{X=0}^{X=L} \\ &= (\widehat{N}_{\mathrm{c}}\delta W)_{X=0}^{X=L} - \Big(\widehat{M}_{\mathrm{c}}\delta W_1 - \frac{\partial\widehat{M}_{\mathrm{c}}}{\partial X}\delta W\Big)_{X=0}^{X=L} + (\widehat{N}_{nc}\delta W_1 - \widehat{M}_{nc}\delta W_2)_{X=0}^{X=L} \\ &\quad - \int_0^L \Big(\frac{\partial\widehat{N}_{\mathrm{c}}}{\partial X} + \frac{\partial^2\widehat{M}_{\mathrm{c}}}{\partial X^2}\Big)\delta W\mathrm{d}X, \end{aligned} \tag{49}$$

in which

$$\widehat{N}_{\mathrm{c}} = N_0W_1 + 2M_{\mathrm{c}}W_1W_2, \quad \widehat{M}_{\mathrm{c}} = M_{\mathrm{c}}, \tag{50a}$$

$$\widehat{N}_{nc} = N_{nc}W_1 + 2M_{nc}W_1W_2, \quad \widehat{M}_{nc} = M_{nc}. \tag{50b}$$

The first variation of external work done by the transverse load is expressed as

$$W_{\mathrm{e}} = \int_0^L Q\delta W\mathrm{d}X. \tag{51}$$

Similarly, we obtain the motion equation

$$\frac{\partial\widehat{N}_{\mathrm{c}}}{\partial X} + \frac{\partial^2\widehat{M}_{\mathrm{c}}}{\partial X^2} - K_1W + K_2W_2 + Q = 0, \tag{52}$$

and the boundary conditions

$$W = 0 \quad \text{or} \quad \widehat{N}_{\mathrm{c}} + \frac{\partial\widehat{M}_{\mathrm{c}}}{\partial X} + K_2W_1 = 0, \tag{53a}$$

$$W_1 = 0 \quad \text{or} \quad \widehat{M}_{\mathrm{c}} - \widehat{N}_{nc} = 0, \tag{53b}$$

$$W_2 = 0 \quad \text{or} \quad \widehat{M}_{nc} = 0. \tag{53c}$$

Substituting Eq. (47) into Eq. (52) yields

$$\begin{aligned}&\frac{EA}{2L}\int_0^L W_1^2\mathrm{d}X\cdot W_2 - EJ(2W_2^3 + 4\,W_1W_2W_3 + W_4) + Q - K_1W_0 \\ &+ K_2W_2EJ(2W_2^2W_6 + 2\,W_1W_3W_6 + 2W_1W_2W_7 + W_8)l^2\eta^2 \\ &\cdot EJ(2\,W_2^2W_4 + 2W_1W_3W_4 + 2W_1W_2W_5 + W_6)(l^2 - \eta^2) = 0. \end{aligned} \tag{54}$$

Neglecting the high-order small quantities and stiffness-softening/hardening size effects, Eq. (54) reduces to the motion equation adopted in the majority of previous literature,

$$Q + K_2W_2 - K_1W_0 + \frac{EA}{2L}\int_0^L W_1^2\mathrm{d}X\cdot W_2 - EJW_4 = 0. \tag{55}$$

Using Eq. (38), Eq. (55) can be normalized as

$$\begin{aligned}&\frac{1}{2}d_3\pi\int_0^1 w_1^2\mathrm{d}x\cdot w_2 - (2\,\pi^2(w_2^3 + 2w_1w_2w_3) + w_4) + \lambda_q + k_2w_2 - k_1w_0 \\ &+ d_5\pi^2(2\,\pi^2(w_2^2w_4 + w_1w_3w_4 + w_1w_2w_5) + w_6)\pi^4d_4 \\ &+ (2\,\pi^2(w_2^2w_6 + w_1w_3w_6 + w_1w_2w_7) + w_8) = 0. \end{aligned} \tag{56}$$

5 Solution procedure

It is well-known that the perturbation method is considered to be one of the most effective ways to deal with boundary-value problems of elastic structures. The main advantage is that the perturbation solutions can accurately satisfy the motion equation and boundary condition in the asymptotic sense. Its reliability and accuracy largely hinge on the choice of small parameter ε which requires to be far smaller than 1 in traditional situation. For a beam with large deflection or deep postbuckling, however, the ratio between the maximum deflection W_{m} and the thickness h may no longer be a small parameter, which leads to the invalidity of the traditional method.

Given the above consideration, Shen and Zhang[62] proposed a two-step perturbation method aming to address the large deformation problems of elastic structures. Its basic solution procedure can be briefly stated as follows. The first step is to introduce a small perturbation parameter ε that may have no physical meaning. The second step takes $B_{11}\varepsilon$ as the second perturbation parameter associated with the dimensionless maximum deflection that may be large in the deflection region or deep postbuckling region, where B_{11} is the amplitude of the first-order term in the perturbation expansion of beam deflection. This approach is successfully used in the nonlinear bending, postbuckling, and nonlinear vibration problems of beams, plates, shells, and even nano-enhanced composites structures[63–65].

In this section, two types of nonlinear problems of nonlocal strain gradient nanobeams are analytically solved by the two-step perturbation method. Taking a simply supported nanobeam with the freely movable end condition as an example, we demonstrate the detailed solution process.

5.1 Nonlinear bending

In this subsection, the static load-maximum deflection relationship is determined. Assume the static load uniformly distributed along the axial direction, i.e., $Q(X,t)=Q_0$. Hence, the governing equation can be rewritten as

$$\begin{aligned}&-\frac{1}{16}\lambda_p w_2(16+24\pi^2 w_1^2+30\pi^4 w_1^4+35\pi^6 w_1^6)+\lambda_q+k_2 w_2-k_1 w_0+\overline{A}_{EJ}^{(8)}w_8+\overline{A}_{EJ}^{(7)}w_7\\&+\overline{A}_{EJ}^{(6)}w_6+\overline{A}_{EJ}^{(5)}w_5+\overline{A}_{EJ}^{(42)}w_4^2+\overline{A}_{EJ}^{(41)}w_4+\overline{A}_{EJ}^{(33)}w_3^3+\overline{A}_{EJ}^{(32)}w_3^2+\overline{A}_{EJ}^{(31)}w_3+\overline{A}_{EJ}^{(27)}w_2^7\\&+\overline{A}_{EJ}^{(25)}w_2^5+\overline{A}_{EJ}^{(23)}w_2^3=0.\end{aligned}\tag{57}$$

We assume

$$w(x,\ \varepsilon)=\sum_{j=1}^{n}\varepsilon^j\varphi_j(x),\quad \lambda_q=\sum_{j=1}^{n}\varepsilon^j\lambda_j,\tag{58}$$

where ε is a small perturbation parameter with no physical meaning. Substituting Eq. (58) into Eq. (57) and equating the coefficients of like powers of ε, we obtain a set of perturbation equations which can be solved step by step.

The first-order perturbation equation is given by

$$\frac{\mathrm{d}^4\varphi_1}{\mathrm{d}x^4}+\lambda_p\frac{\mathrm{d}^2\varphi_1}{\mathrm{d}x^2}+k_1\varphi_1-k_2\frac{\mathrm{d}^2\varphi_1}{\mathrm{d}x^2}-\pi^2\Big(d_5\frac{\mathrm{d}^6\varphi_1}{\mathrm{d}x^6}+d_4\pi^2\frac{\mathrm{d}^8\varphi_1}{\mathrm{d}x^8}\Big)-\lambda_1=0.\tag{59}$$

With consideration of the simply supported boundary conditions, the solution to Eq. (59) may be expressed as

$$\varphi_1=B_{11}\sin(mx).\tag{60}$$

Substituting Eq. (60) into Eq. (59) and applying the Galerkin procedure, one has

$$\lambda_1=-\frac{1}{4}B_{11}m\pi(\pi^2m^6(d_4\pi^2m^2-d_5)+\lambda_p m^2-(k_1+k_2m^2+m^4)).\tag{61}$$

Using Eqs. (60) and (61), the simplified second-order perturbation equation is

$$\frac{\mathrm{d}^4\varphi_2}{\mathrm{d}x^4}+\lambda_p\frac{\mathrm{d}^2\varphi_2}{\mathrm{d}x^2}+k_1\varphi_2-k_2\frac{\mathrm{d}^2\varphi_2}{\mathrm{d}x^2}-\pi^2\Big(d_5\frac{\mathrm{d}^6\varphi_2}{\mathrm{d}x^6}+d_4\pi^2\frac{\mathrm{d}^8\varphi_2}{\mathrm{d}x^8}\Big)-\lambda_2=0. \tag{62}$$

Accordingly, φ_2 is taken as the following form:

$$\varphi_2=B_{22}\sin(2mx). \tag{63}$$

Substituting Eq. (63) into Eq. (62) yields

$$\lambda_2=0,\quad B_{22}=0. \tag{64}$$

Using the first two order solutions, the reduced form of the third-order equation is

$$\frac{\mathrm{d}^4\varphi_3}{\mathrm{d}x^4}+\lambda_p\frac{\mathrm{d}^2\varphi_3}{\mathrm{d}x^2}+k_1\varphi_3-k_2\frac{\mathrm{d}^2\varphi_3}{\mathrm{d}x^2}-\pi^2\Big(d_5\frac{\mathrm{d}^6\varphi_3}{\mathrm{d}x^6}+d_4\pi^2\frac{\mathrm{d}^8\varphi_3}{\mathrm{d}x^8}\Big)$$

$$+(f_{31}\sin(mx)+f_{33}\sin(3mx))B_{11}^3-\lambda_3=0, \tag{65}$$

where

$$f_{31}=-\frac{1}{8}\pi^2m^4(4m^2(m^4\pi^4d_4-m^2\pi^2d_5-1)+3\lambda_p), \tag{66a}$$

$$f_{33}=-\frac{3}{8}\pi^2m^4(4m^2(61m^4\pi^4d_4-7m^2\pi^2d_5-1)+\lambda_p). \tag{66b}$$

The right-hand side of Eq. (65) suggests seeking φ_3 in the form of

$$\varphi_3=B_{31}\sin(mx)+B_{33}\sin(3mx). \tag{67}$$

Substituting Eq. (67) into Eq. (65) yields

$$B_{31}=0,\quad B_{33}=B_{11}^3\gamma_{33},\quad \lambda_3=\frac{1}{4}m\pi f_{31}B_{11}^3, \tag{68}$$

where

$$\gamma_{33}=\frac{f_{33}}{729\pi^2m^6(9\pi^2m^2d_4-d_5)-(81m^4+9m^2k_2-9m^2\lambda_p+k_1)}. \tag{69}$$

Similar to the previous steps, the fourth-order equation after simplification is

$$\frac{\mathrm{d}^4\varphi_4}{\mathrm{d}x^4}+\lambda_p\frac{\mathrm{d}^2\varphi_4}{\mathrm{d}x^2}+k_1\varphi_4-k_2\frac{\mathrm{d}^2\varphi_4}{\mathrm{d}x^2}-\pi^2\Big(d_5\frac{\mathrm{d}^6\varphi_4}{\mathrm{d}x^6}+d_4\pi^2\frac{\mathrm{d}^8\varphi_4}{\mathrm{d}x^8}\Big)-\lambda_4=0. \tag{70}$$

Obviously, φ_4 is taken to be the following form:

$$\varphi_4=B_{44}\sin(4mx). \tag{71}$$

Substituting Eq. (71) into Eq. (70) leads to

$$B_{44}=0,\quad \lambda_4=0. \tag{72}$$

The fifth-order equation through properly manipulation is given by

$$\frac{\mathrm{d}^4\varphi_5}{\mathrm{d}x^4}+\lambda_p\frac{\mathrm{d}^2\varphi_5}{\mathrm{d}x^2}+k_1\varphi_5-k_2\frac{\mathrm{d}^2\varphi_5}{\mathrm{d}x^2}-\pi^2\Big(d_5\frac{\mathrm{d}^6\varphi_5}{\mathrm{d}x^6}+d_4\pi^2\frac{\mathrm{d}^8\varphi_5}{\mathrm{d}x^8}\Big)$$

$$+(f_{51}\sin(mx)+f_{53}\sin(3mx)+f_{55}\sin(5mx))B_{11}^5-\lambda_5=0, \tag{73}$$

in which

$$f_{51} = -\frac{9}{8}\pi^2 m^4 \gamma_{33}(4m^2(61m^4\pi^4 d_4 - 7m^2\pi^2 d_5 - 1) + \lambda_p) + \frac{3}{64}m^6\pi^4(8m^2(11\pi^4 m^4 d_4 - 2\pi^2 m^2 d_5 - 1) + 5\lambda_p), \tag{74a}$$

$$f_{53} = \frac{9}{4}\pi^2 m^4(4m^2(5 - 365\pi^4 m^4 d_4 + 41\pi^2 m^2 d_5) - 3\lambda_p)\gamma_{33} - \frac{3}{128}\pi^4 m^6(8m^2(397\pi^4 m^4 d_4 - 46\pi^2 m^2 d_5 - 7) + 15\lambda_p), \tag{74b}$$

$$f_{55} = -\frac{45}{8}\pi^2 m^4(4m^2(1\ 363m^4\pi^4 d_4 - 59m^2\pi^2 d_5 - 3) + \lambda_p)\gamma_{33} - \frac{15}{128}\pi^4 m^6(8m^2(411m^4\pi^4 d_4 - 16m^2\pi^2 d_5 - 1) + \lambda_p). \tag{74c}$$

The form of the terms on the right-hand side of Eq. (73) suggests seeking φ_5 as

$$\varphi_5 = B_{51}\sin(mx) + B_{53}\sin(3mx) + B_{55}\sin(5mx). \tag{75}$$

Substituting Eq. (75) into Eq. (73), we obtain

$$B_{51} = 0, \quad B_{53} = B_{11}^5\gamma_{53}, \quad B_{55} = B_{11}^5\gamma_{55}, \quad \lambda_5 = \frac{1}{4}B_{11}^5 f_{51} m\pi, \tag{76}$$

where

$$\gamma_{53} = \frac{f_{53}}{729\pi^2 m^6(9\pi^2 m^2 d_4 - d_5) - (k_1 + 9m^2 k_2 + 81m^4 - 9\lambda_p m^2)}, \tag{77a}$$

$$\gamma_{55} = \frac{f_{55}}{15\ 625\pi^2 m^6(25\pi^2 m^2 d_4 - d_5) - (k_1 + 25m^2 k_2 + 625m^4 - 25\lambda_p m^2)}. \tag{77b}$$

Using the above solutions, the sixth-order perturbation equation is

$$\frac{\mathrm{d}^4\varphi_6}{\mathrm{d}x^4} + \lambda_p\frac{\mathrm{d}^2\varphi_6}{\mathrm{d}x^2} + k_1\varphi_6 - k_2\frac{\mathrm{d}^2\varphi_6}{\mathrm{d}x^2} - \pi^2\Big(d_5\frac{\mathrm{d}^6\varphi_6}{\mathrm{d}x^6} + d_4\pi^2\frac{\mathrm{d}^8\varphi_6}{\mathrm{d}x^8}\Big) - \lambda_6 = 0. \tag{78}$$

Similarly, φ_6 is assumed to be

$$\varphi_6 = B_{66}\sin(6mx). \tag{79}$$

Substituting Eq. (79) into Eq. (78) leads to

$$B_{66} = 0, \quad \lambda_6 = 0. \tag{80}$$

The seventh-order equation is readily obtained as

$$\frac{\mathrm{d}^4\varphi_7}{\mathrm{d}x^4} + \lambda_p\frac{\mathrm{d}^2\varphi_7}{\mathrm{d}x^2} + k_1\varphi_7 - k_2\frac{\mathrm{d}^2\varphi_7}{\mathrm{d}x^2} - \pi^2\Big(d_5\frac{\mathrm{d}^6\varphi_7}{\mathrm{d}x^6} + d_4\pi^2\frac{\mathrm{d}^8\varphi_7}{\mathrm{d}x^8}\Big) + (f_{71}\sin(mx) + f_{73}\sin(3mx) + f_{75}\sin(5mx) + f_{77}\sin(7mx))B_{11}^7 - \lambda_7 = 0, \tag{81}$$

where

$$
\begin{aligned}
f_{71} = &-\frac{9}{4}\pi^2 m^4(4m^4\pi^2(365\,m^2\pi^2 d_4 - 41 d_5) + 3\,\lambda_p - 20m^2)\gamma_{33}^2 \\
&- \frac{15}{128}\pi^4 m^6(8\pi^2 m^4(397 m^2\pi^2 d_4 - 46\,d_5) + (15\,\lambda_p - 56m^2))\gamma_{33} \\
&- \frac{1}{1\ 024}\pi^6 m^8(64\pi^2 m^4(95\pi^2 m^2 d_4 - 14 d_5) + 5(35\lambda_p - 64\,m^2)) \\
&- \frac{9}{8}\pi^2 m^4(\,4m^4\pi^2(61\,m^2\pi^2 d_4 - 7 d_5) + \lambda_p - 4\,m^2)\gamma_{53}, \qquad (82a)\\
f_{73} = &-\frac{27}{64}\pi^4 m^6(8\pi^2 m^4(1\ 321\,\pi^2 m^2 d_4 - 102 d_5) + (15\,\lambda_p - 88m^2))\gamma_{33} \\
&- \frac{9}{4}\pi^2 m^4(4\pi^2 m^4(365\pi^2 m^2 d_4 - 41\,d_5) + (3\lambda_p - 20m^2))\gamma_{53} \\
&- \frac{45}{8}\,\pi^2 m^4(4m^4\pi^2(1\ 363 m^2\pi^2 d_4 - 59\,d_5) + \lambda_p - 12m^2)\gamma_{55} \\
&- \frac{9}{1\ 024}\pi^6 m^8(128\pi^2 m^4(76\,\pi^2 m^2 d_4 - 7 d_5) + (35\lambda_p - 128m^2)), \qquad (82b)\\
f_{75} = &-\frac{45}{8}\pi^2 m^4(\,4m^4\pi^2(4\ 271 m^6 d_4\pi^4 - 197 d_5) + 3\,\lambda_p - 44\,m^2)\gamma_{33}^2 \\
&- \frac{15}{32}\pi^4 m^6(8\pi^2 m^4(8\ 209\pi^2 m^2 d_4 - 358 d_5) + (15\,\lambda_p - 152\,m^2))\gamma_{33} \\
&- \frac{45}{8}\pi^2 m^4(4m^4\pi^2(1\ 363 m^2\pi^2 d_4 - 59 d_5) + \lambda_p - 12\,m^2)\gamma_{53} \\
&- \frac{25}{4}\pi^2 m^4(4\pi^2 m^4(7\ 813\,\pi^2 m^2 d_4 - 313 d_5) + (3\,\lambda_p - 52m^2))\gamma_{55} \\
&- \frac{5}{1\ 024}\pi^6 m^8(128\pi^2 m^4(797\pi^2 m^2 d_4 - 35 d_5) + (35\,\lambda_p - 256\,m^2)), \qquad (82c)\\
f_{77} = &-\frac{63}{8}\pi^2 m^4(4m^4\pi^2(29\ 777 m^2\pi^2 d_4 - 641 d_5) + 3\lambda_p - 68\,m^2)\gamma_{33}^2 \\
&- \frac{21}{128}m^6\pi^4(8\,m^4\pi^2(48\ 421 m^2\pi^2 d_4 - 1\ 102 d_5) + 15\,\lambda_p - 248m^2)\gamma_{33} \\
&- \frac{35}{8}\pi^2 m^4(4m^4\pi^2(33\ 319\,m^2\pi^2 d_4 - 757 d_5) + 3\,\lambda_p - 76m^2)\gamma_{55} \\
&- \frac{7}{1\ 024}\pi^6 m^8(\,64m^4\pi^2(1\ 471 m^2\pi^2 d_4 - 34 d_5) + 5\,\lambda_p - 64\,m^2). \qquad (82d)
\end{aligned}
$$

The seventh-order perturbation solution φ_7 takes the form of

$$\varphi_7 = B_{71}\sin(mx) + B_{73}\sin(3mx) + B_{75}\sin(5mx) + B_{77}\sin(7mx). \qquad (83)$$

Substituting Eq. (83) into Eq. (81) yields

$$B_{71} = 0, \quad B_{73} = B_{11}^7\gamma_{73}, \quad B_{75} = B_{11}^7\gamma_{75}, \quad B_{77} = B_{11}^7\gamma_{77}, \quad \lambda_7 = \frac{1}{4}B_{11}^6 f_{71} m\pi, \qquad (84)$$

where

$$\gamma_{73} = \frac{f_{73}}{729\pi^2 m^6(9\pi^2 m^2 d_4 - d_5) - (k_1 + 9\,m^2 k_2 + 81m^4 - 9\lambda_p m^2)}, \qquad (85a)$$

$$\gamma_{75} = \frac{f_{75}}{15\ 625\pi^2 m^6(25\pi^2 m^2 d_4 - d_5) - (k_1 + 25\,m^2 k_2 + 625m^4 - 25\lambda_p m^2)}, \qquad (85b)$$

$$\gamma_{77} = \frac{f_{77}}{117\ 649\pi^2 m^6(49\pi^2 m^2 d_4 - d_5) - (k_1 + 49\,m^2 k_2 + 2\ 401m^4 - 49\lambda_p m^2)}. \qquad (85c)$$

Given the above, the asymptotic solutions of the deflection and static load are expressed as

$$w = \varepsilon B_{11}\sin(mx) + (\varepsilon B_{11})^3\gamma_{33}\sin(3mx) + (\varepsilon B_{11})^5(\gamma_{53}\sin(3mx) + \gamma_{55}\sin(5mx)) + (\varepsilon B_{11})^7(\gamma_{73}\sin(3mx) + \gamma_{75}\sin(5mx) + \gamma_{77}\sin(7mx)), \tag{86a}$$

$$\lambda_q = \frac{1}{4}m\pi(\varepsilon B_{11}(m^6\pi^2(d_5 - m^2\pi^2 d_4) + (k_1 + k_2m^2 + m^4 - m^2\lambda_p)) + (\varepsilon B_{11})^3 f_{31} + (\varepsilon B_{11})^5 f_{51} + (\varepsilon B_{11})^7 f_{71}). \tag{86b}$$

In Eqs. (86a) and (86b), εB_{11} will be taken as the second perturbation parameter relating to the dimensionless maximum deflection w_{m}. Substituting $x = \pi/(2m)$ into Eq. (86a) yields

$$w_{\mathrm{m}} = w\Big(\frac{\pi}{2m}\Big) = \varepsilon B_{11} - (\varepsilon B_{11})^3\gamma_{33} - (\varepsilon B_{11})^5(\gamma_{53} - \gamma_{55}) - (\varepsilon B_{11})^7(\gamma_{73} - \gamma_{75} + \gamma_{77}). \tag{87}$$

From Eq. (87), εB_{11} can be expressed in an explicit form as

$$\varepsilon B_{11} = w_{\mathrm{m}} + w_{\mathrm{m}}^3 h_3 + h_5 w_{\mathrm{m}}^5 + h_5 w_{\mathrm{m}}^7 + O(w_{\mathrm{m}}^9), \tag{88}$$

where

$$h_3 = \gamma_{33}, \quad h_5 = 3\gamma_{33}^2 - \gamma_{55} + \gamma_{53}, \quad h_7 = 12\gamma_{33}^3 + 8\gamma_{33}(\gamma_{53} - \gamma_{55}) + (\gamma_{73} - \gamma_{75} + \gamma_{77}). \tag{89}$$

Substituting Eq. (88) into Eq. (86b) yields the following static load-deflection relationship:

$$\begin{aligned}\lambda_q = {} & (m^6\pi^2(d_5 - m^2\pi^2 d_4) + (k_1 + k_2m^2 + m^4 - m^2\lambda_p))w_{\mathrm{m}} \\ & \cdot (f_{31} + m^6\pi^2 h_3(d_5 - m^2\pi^2 d_4) + h_3(k_1 + m^2k_2 + m^4 - m^2\lambda_p))w_{\mathrm{m}}^3 \\ & \cdot (f_{51} + 3f_{31}h_3 + m^6\pi^2 h_5(d_5 - m^2\pi^2 d_4) + h_5(k_1 + m^2k_2 + m^4 - m^2\lambda_p))w_{\mathrm{m}}^5 \\ & \cdot (f_{71} + 3f_{31}(h_5 + h_3^2) + 5f_{51}h_3 + m^6\pi^2 h_7(d_5 - m^2\pi^2 d_4) \\ & + h_7(k_1 + m^2k_2 + m^4 - m^2\lambda_p))w_{\mathrm{m}}^7.\end{aligned} \tag{90}$$

5.2 Postbuckling

In this subsection, the postbuckling equilibrium path of a simply supported nanobeam subject to an axial compression is seeked by the two-step perturbation method. For the present case, $\lambda_q = 0$, and w is only a function of x. Equation (39) is rewritten as

$$\begin{aligned}& -\frac{1}{16}\lambda_p w_2(16 + 24\pi^2 w_1^2 + 30\pi^4 w_1^4 + 35\pi^6 w_1^6) + k_2 w_2 - k_1 w_0 + \overline{A}_{EJ}^{(8)} w_8 + \overline{A}_{EJ}^{(7)} w_7 + \overline{A}_{EJ}^{(6)} w_6 \\ & + \overline{A}_{EJ}^{(5)} w_5 + \overline{A}_{EJ}^{(42)} w_4^2 + \overline{A}_{EJ}^{(41)} w_4 + \overline{A}_{EJ}^{(33)} w_3^3 + \overline{A}_{EJ}^{(32)} w_3^2 + \overline{A}_{EJ}^{(31)} w_3 + \overline{A}_{EJ}^{(27)} w_2^7 + \overline{A}_{EJ}^{(25)} w_2^5 \\ & + \overline{A}_{EJ}^{(23)} w_2^3 = 0.\end{aligned} \tag{91}$$

Unlike the nonlinear bending, λ_p is now an unknown. The deflection and compression are assumed as

$$w(x,\ \varepsilon) = \sum_{j=1}^{n} \varepsilon^j \varphi_j(x), \quad \lambda_p = \sum_{j=0}^{n} \varepsilon^j \lambda_j. \tag{92}$$

Similar to the case of nonlinear bending, up to seventh-order perturbation equations are solved as the postbuckling solution is needed. Substituting Eq. (92) into Eq. (91) and equating

coefficients of such powers of ε, a set of perturbation equations can be obtained. The asymptotic solutions to Eq. (91) may be expressed by

$$w = \varepsilon B_{11}\sin(mx) + (\varepsilon B_{11})^3\gamma_{33}\sin(3mx) + (\varepsilon B_{11})^5(\gamma_{53}\sin(3mx) + \gamma_{55}\sin(5mx)) + (\varepsilon B_{11})^7(\gamma_{73}\sin(3mx) + \gamma_{75}\sin(5mx) + \gamma_{77}\sin(7mx)), \tag{93a}$$

$$\lambda_p = \lambda_0 + \frac{(\varepsilon B_{11})^2 f_{31}}{m^2} + \frac{(\varepsilon B_{11})^4 f_{51}}{m^2} + \frac{(\varepsilon B_{11})^6 f_{71}}{m^2}, \tag{93b}$$

where the terms λ_0, f_{31}, f_{51}, f_{71}, γ_{33}, γ_{53}, γ_{55}, γ_{73}, γ_{75}, and γ_{77} are listed in detail in Appendix A. Treating εB_{11} as the second perturbation parameter, we obtain the following postbuckling equilibrium path:

$$\lambda_p = m^2 + \frac{k_1}{m^2} + k_2 + m^4\pi^2(d_5 - m^2\pi^2 d_4) + \frac{f_{31}w_{\mathrm{m}}^2}{m^2} + \frac{(f_{51} + 2f_{31}h_3)w_{\mathrm{m}}^4}{m^2} + \frac{(2f_{31}h_5 + f_{31}h_3^2 + f_{71} + 4f_{51}h_3)w_{\mathrm{m}}^6}{m^2}. \tag{94}$$

For the case of fully immovable end condition, the perturbation solution of nonlinear bending is presented in Appendix B.

6 Numerical results and discussion

6.1 Convergence study

The objective of this subsection is to verify the convergence of asymptotic solutions by taking the nonlinear bending and postbuckling of nanobeams as examples. Accordingly, it is essential to determine how many high-order terms of the maximum deflection w_{m} need to be retained in the static load-deflection curve and postbuckling equilibrium path.

Figure 2 displays the relationship between the postbuckling load versus the maximum deflection for a simply supported nanobeam without elastic foundation when different high-order terms of maximum deflection are truncated. As demonstrated in this figure, the postbuckling load nonlinearly increases with the increase in the maximum deflection, and this trend is especially noticeable for large values of the maximum deflection. In addition, the high-order terms play an increasingly important role in the postbuckling equilibrium path while the maximum deflection increases. To guarantee the convergence of the asymptotic solution of the postbuckling equilibrium path, it needs to keep terms up to $O(w_{\mathrm{m}}^2)$ when $w_{\mathrm{m}} \leqslant 0.15$ and $O(w_{\mathrm{m}}^6)$ when w_{m} increases up to 0.3.

Figure 3 illustrates the variation of the postbuckling load with the maximum deflection for a simply supported nanobeam resting on an elastic foundation with truncating nonlinear terms up to different orders. It should be pointed out that the buckling mode maybe jumps as the elastic foundation stiffnesses increase to some certain values. The linear buckling load $\lambda_p^{(\mathrm{L})}$ for a nanobeam with a two-parameter elastic foundation is given as

$$\lambda_p^{(\mathrm{L})} = \min\left\{m^2 + \frac{k_1}{m^2} + k_2 + \frac{\pi^2 m^4}{L^2}\left((l^2 - \eta^2) - \frac{m^2\pi^2 l^2\eta^2}{L^2}\right)\right\}, \quad m = 1,\ 2,\ 3,\ \cdots, \tag{95}$$

in which the foundation parameters $(k_1,\ k_2)$ along with the nonlocal strain parameters $(l,\ \eta)$ have obvious influence on the buckling behavior of nanobeams. For a given positive number k_1, the linear buckling load is determined as

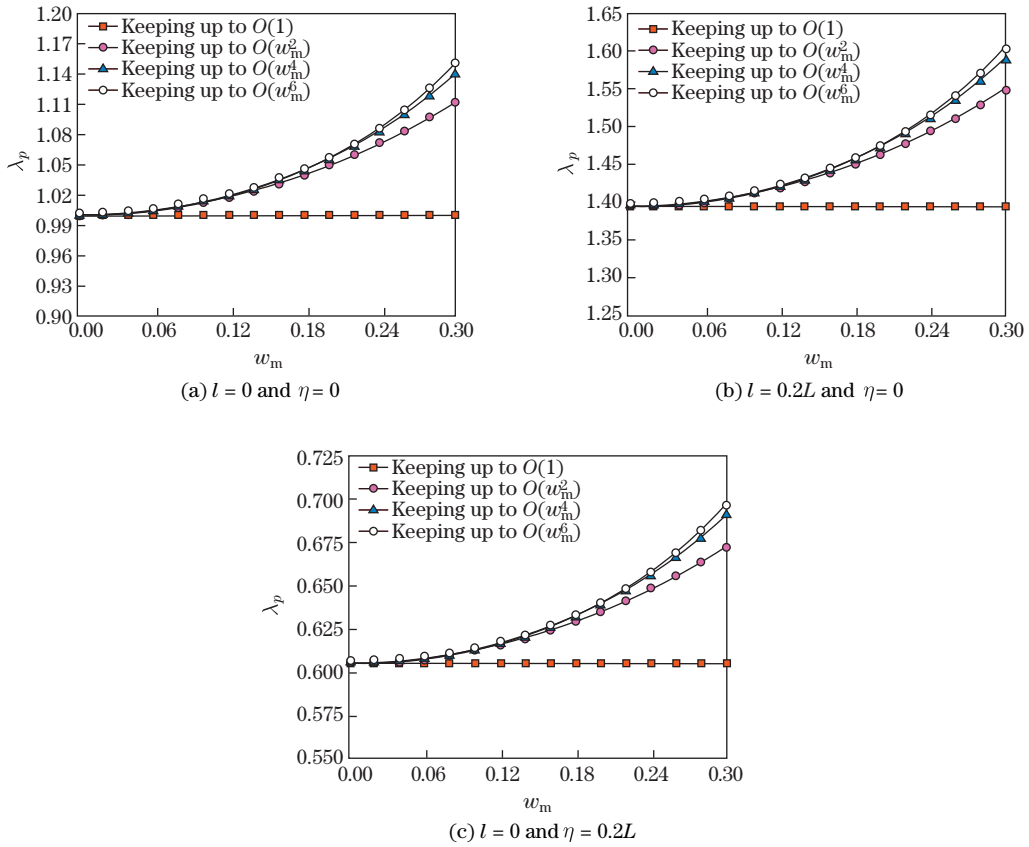

Fig. 2 Convergence of postbuckling equilibrium path for simply supported nanobeam without any elastic foundation ($k_1 = k_2 = 0$ and $m = 1$)

$$\lambda_p^{(\mathrm{L})} = \begin{cases} m^2 + \dfrac{k_1}{m^2} + k_2 + \dfrac{\pi^2 m^4}{L^2}\left((l^2-\eta^2) - \dfrac{m^2\pi^2 l^2\eta^2}{L^2}\right), & m^2(m-1)^2 < k_1 < m^2(m+1)^2, \\ m^2 + (m+1)^2 + k_2 + \dfrac{\pi^2 m^4}{L^2}\left((l^2-\eta^2) - \dfrac{m^2\pi^2 l^2\eta^2}{L^2}\right), & k_1 = m^2(m+1)^2. \end{cases} \tag{96}$$

Obviously, the beam without any foundation and size effect is buckled with $m = 1$. For the current example, the buckling occurs at the second mode. One can observe that the postbuckling equilibrium paths tend to be convergent by increasing the high-order term of the maximum deflection, and acceptable results are obtained by keeping the terms up to $O(w_{\mathrm{m}}^6)$ for the large deflection regime (e.g., $w_{\mathrm{m}} = 0.3$).

Figures 4 and 5 investigate the convergence of two-step perturbation method in dealing with the nonlinear bending problem of nanobeams for keeping up to different orders of nonlinear terms. The ranges of values of the maximum deflection are set to be [0, 0.3] for the movable end condition. Similar to the observations in Figs. 2 and 3, the transverse load nonlinearly increases with the deflection. Meanwhile, the load-deflection curves tend to be stable with retaining more high-order nonlinear terms in asymptotic solutions whether for movable or immovable beam models. In addition, it can be observed that the asymptotic solution of load-deflection relationship needs to keep terms up to $O(w_{\mathrm{m}}^3)$ when $w_{\mathrm{m}} \leqslant 0.15$, $O(w_{\mathrm{m}}^7)$ when w_{m} approaches 0.3 for movable nanobeams, and keep terms up to $O(w_{\mathrm{m}}^3)$ for immovable nanobeams to ensure good accuracy.

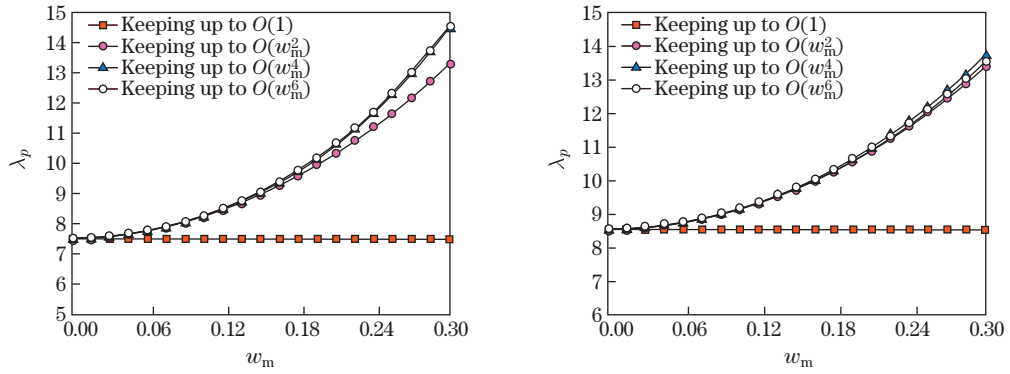

(a) $l = 0$ and $\eta = 0$ (b) $l = 0.1L$ and $\eta = 0.5L$

Fig. 3 Convergence of postbuckling load for simply supported nanobeam with elastic foundation ($k_1 = 10, k_2 = 1$, and $m = 2$)

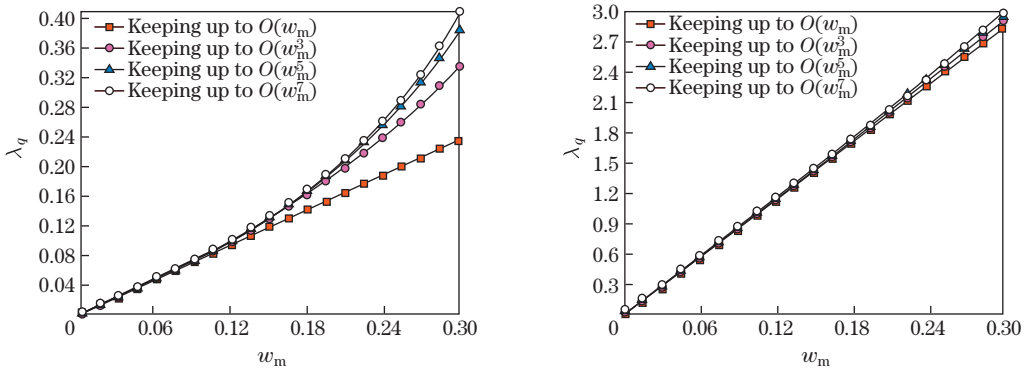

(a) $k_1 = k_2 = 0$, $l = 0$, and $\eta = 0$ (b) $k_1 = 10$, $k_2 = 1$, $l = 0.1L$, and $\eta = 0.5L$

Fig. 4 Convergence of load-deflection curves for movable nanobeam with or without elastic foundation ($m = 1$)

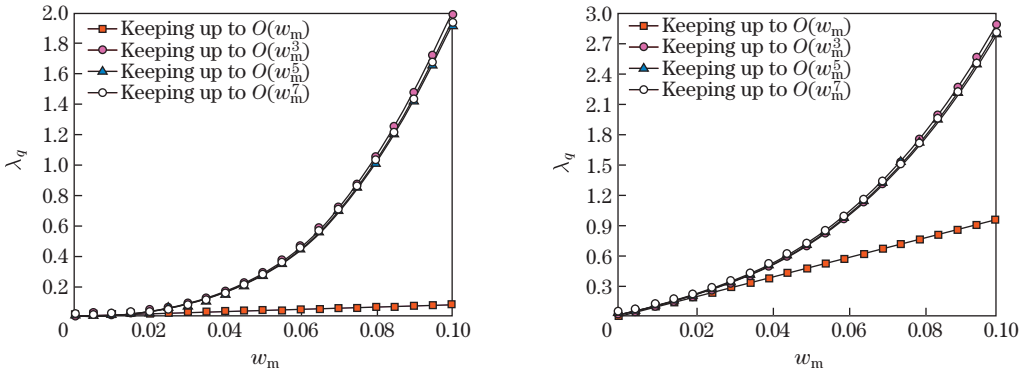

(a) $k_1 = k_2 = 0$, $l = 0$, and $\eta = 0$ (b) $k_1 = k_2 = 0$, $l = 0.1L$, $\eta = 0.05L$, and $L = 100R$, where R is radius of gyration of cross-section

Fig. 5 Convergence of load-deflection curves for immovable nanobeam with or without elastic foundation ($m = 1$)

To emphasize an important point, the maximum deflection should be limited in a relatively small range when performing nonlinear bending analysis on the nanobeams with an immovable end. The reason for this is that the influence of contraction of cross-section will become obvious when the deflection has a relatively large value. In what follows, the maximum deflection is assumed not to exceed 0.1 for this case.

6.2 Comparison study

In order to establish the authenticity of the present work, several numerical examples are proposed for the nonlinear bending and postbuckling of beams at macro/micro-scopic. Direct comparison is conducted between the present results and those in the literature[36,59,66–69].

Table 1 calculates the dimensionless buckling loads for a simply supported beam resting on an elastic foundation and compares them with the results from Kien[66], Naidu and Rao[67], and Shen[59]. The geometry, material, and foundation parameters used here are $L = 5$ m, $J = 1.0 \times 10^{-5}$ m^4, $E = 210$ GPa, $k_1 = K_1L^4/(EJ)$, and $k_2 = K_2L^2/(\pi^2EJ)$. It is observed that our results are consistent with those in the literature. Table 2 presents the postbuckling loads for a simply supported beam without foundation under different values of the maximum deflection, and the results reported by Timoshenko and Gere[68] and Shen[59] in which the elliptic function and two-step perturbation methods were used, respectively. It can be seen that the two-step perturbation solution of Shen[59] and the present one agree well with the elliptic function solution when $w_{\rm m} \leqslant 0.3$. The differences of the two methods increase gradually with the increase in the maximum deflection, but it remains acceptable even when $w_{\rm m} = 0.381\ 5$ where the relative error is about 6.8%.

Table 1 Comparison of buckling loads for simply supported beam with elastic foundation

(k_1, k_2)	Kien[66]	Naidu and Rao[67]	Shen[59]	Present
(0, 0)	9.902 3	9.869 6	9.869 6	9.869 6
(1, 0)	10.003 4	9.970 9	9.970 9	9.970 9
(100, 0)	20.009 5	20.002 0	20.001 7	20.001 7
(100, 0.5)	24.933 1	24.937 0	24.936 5	24.936 5
(100, 2.5)	44.488 4	44.676 0	44.675 7	44.675 7

Table 2 Comparison of postbuckling load for simply supported beam without foundation

$w_{\rm m}$	λ_p		
	Exact solutions[68]	Shen[59]	Present
0.000 0	1.000	1.000	1.000 0
0.055 5	1.004	1.004	1.003 8
0.109 5	1.015	1.016	1.015 3
0.162 0	1.035	1.036	1.035 1
0.211 0	1.064	1.067	1.063 3
0.256 5	1.102	1.107	1.100 7
0.296 5	1.151	1.154	1.145 6
0.331 5	1.215	1.207	1.197 3
0.339 5	1.294	1.221	1.249 2
0.381 5	1.393	1.304	1.298 1

Figure 6 compares the present postbuckling load-deflection curves with those of Shen[59] for a simply supported beam with or without elastic foundation. The finite depth elastic foundation stiffnesses K_1 and K_2 are determined by the Vlasov formulae. The geometric and material parameters used are $K_1 = 26.6$ MPa/m and $K_2 = 5.8$ MPa/m before nondimensionalizing or $k_1 = 9.49$ and $k_2 = 0.82$ after nondimensionalizing. As stated before, the order of buckling mode

depends on the Winkler foundation stiffness. In the present example, the beams with or without foundation buckle with $m = 2$ and $m = 1$, respectively. It can be observed that our results agree well with those reported in the literature.

Figure 7 conducts a comparison between the present load-deflection curves and those of Shen[59] and Horibe and Asano[69], where $R = \sqrt{J/A}$ is the radius of gyration of cross-section, $L/R = 100$, $k_1 = K_1 L^4/(EJ)$, and $k_2 = K_2 L^2/(EJ)$. Excellent agreement is observed for both movable and immovable beams.

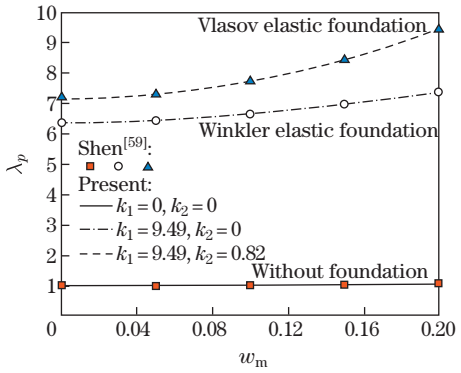

Fig. 6 Comparison of postbuckling equilibrium paths for simply supported beam with or without elastic foundation (color online)

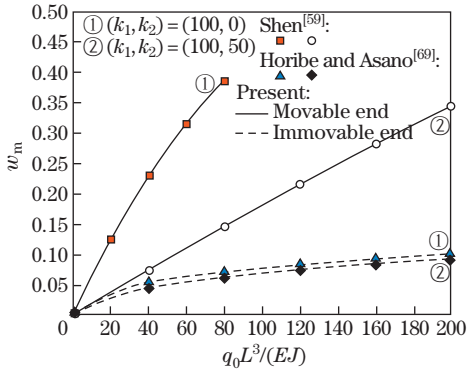

Fig. 7 Comparison of static load-deflection curves for simply supported beam with or without elastic foundation for $L/R = 100$ (color online)

Note that the aforementioned comparison examples involve the macroscopic structures only. However, there are few studies on large deflected size-dependent nanobeams. On account of this, the present results are limited to compare with those of Shen and Zhang[36] who developed a nonlocal beam model incorporating large deflection to analyze the nonlinear mechanical behaviors of SWCNTs on a finite depth elastomeric substrate. The effective material properties of SWCNTs and substrate were given in Ref. [36]. Table 3 presents the linear buckling loads for three kinds of SWCNTs under different temperatures and nonlocal parameters. The integer numbers in the parentheses indicate the corresponding buckling mode. It can be observed that the present model can achieve results consistent with those reported in the literature for the smaller nonlocal parameter, while there may be obvious difference between the two for the larger nonlocal parameter especially for the case of (17, 0)-CNT. Part of the reason may lie in the fact that the present model neglects the nonlinear terms higher than second order in the asymptotic expression of the nonlocal constitutive equation. It should be noted that the buckling modes and critical buckling loads provided by Shen and Zhang[36] maybe have some erroneous and the verification of this point is tagged with an underline.

Figure 8 displays the postbuckling load-deflection curves for a (12, 12)-SWCNT resting on an elastic foundation under three kinds of temperature. It can be seen that the postbuckling load is reduced and increases with the increase in the temperature and maximum deflection, respectively, and there exhibits distinct difference between the present model and that proposed by Shen and Zhang[36] although there is a similar variation tendency.

6.3 Postbuckling

In this and the next subsection, we take SWCNTs resting on an elastomeric substrate as examples, and investigate their postbuckling and nonlinear bending behaviors.

Figure 9 exhibits the variation of critical buckling loads with the nonlocal and strain gradient parameters as well as the foundation stiffness parameters. As seen from this figure, as the nonlocal parameter decreases or the strain gradient and elastic foundation parameters increase,

the critical buckling loads increase. This indicates that the nonlocal effect weakens the post-buckling resistance of small scale structures, while the strain gradient effect does the opposite. The buckling stability is enhanced by increasing the foundation stiffnesses. Additionally, the buckling mode is obviously affected by the Winkler foundation parameter K_1 and jumps at some special values (see also Eq. (96)).

Table 3 Comparison of linear buckling loads for SWCNTs resting on elastomeric substrate

T/K	e_0a	(12, 12)-tube		(10, 10)-tube		(17, 0)-tube	
		Shen and Zhang[36]	Present	Shen and Zhang[36]	Present	Shen and Zhang[36]	Present
300	0	18.986(3)	19.017(3)	16.029(3)	16.064(3)	12.735(3)	12.790(3)
	2	18.558(3)	18.566(3)	15.514(3)	15.509(3)	12.434(3)	12.463(3)
	4	17.500(3)	17.211(3)	14.332(3)	13.842(3)	11.303(4)	11.484(4)
500	0	15.500(3)	15.528(3)	13.162(3)	13.196(3)	10.046(3)	10.087(3)
	2	15.084(3)	15.089(3)	12.685(3)	12.652(3)	9.747(3)	9.762(3)
	4	14.055(3)	13.771(3)	11.500(3)	11.019(3)	9.064(3)	8.787(3)
700	0	10.295(2)	10.309(2)	8.685(3)	8.704(2)	7.269(2)	7.297(2)
	2	10.211(2)	10.223(2)	8.582(3)	8.598(2)	7.049(2)	7.233(2)
	4	9.981(2)	9.965(2)	8.311(3)	8.279(2)	6.371(3)	6.085(3)

The number in parentheses denotes buckling mode (m) in X-direction

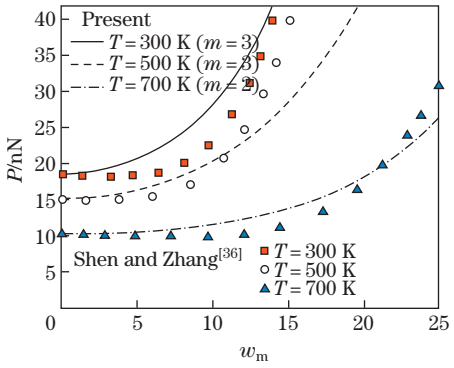

Fig. 8 Comparison of postbuckling equilibrium paths of SWCNTs resting on elastic foundation for (12,12)-tube (color online)

Figure 10 demonstrates the two kinds of size effects on the postbuckling equilibrium paths of SWCNTs on an elastomeric substrate at room temperature. Three different types of SWCNTs, namely, armchair (12, 12) and (10, 10)-tubes and zigzag (17, 0)-tube, are considered. According to Eq. (96), it can be concluded that the above SWCNTs resting on elastomeric substrates are buckled with $m = 3$. This figure shows that the postbuckling loads take on the nonlinearly increasing trend as the maximum deflections raise especially for the relatively large deflection. Besides, the (17, 0)-CNT is more prone to be buckled, the (10, 10)-CNT does less, and the (12, 12)-CNT does least, which indicates that the bending rigidity of (17, 0)-CNT is the largest, and (10, 10)-CNT and (12, 12)-CNT are followed. Comparing the three subfigures, it can also be observed that the postbuckling equilibrium paths may be more affected by the nonlocal parameter than the strain gradient one.

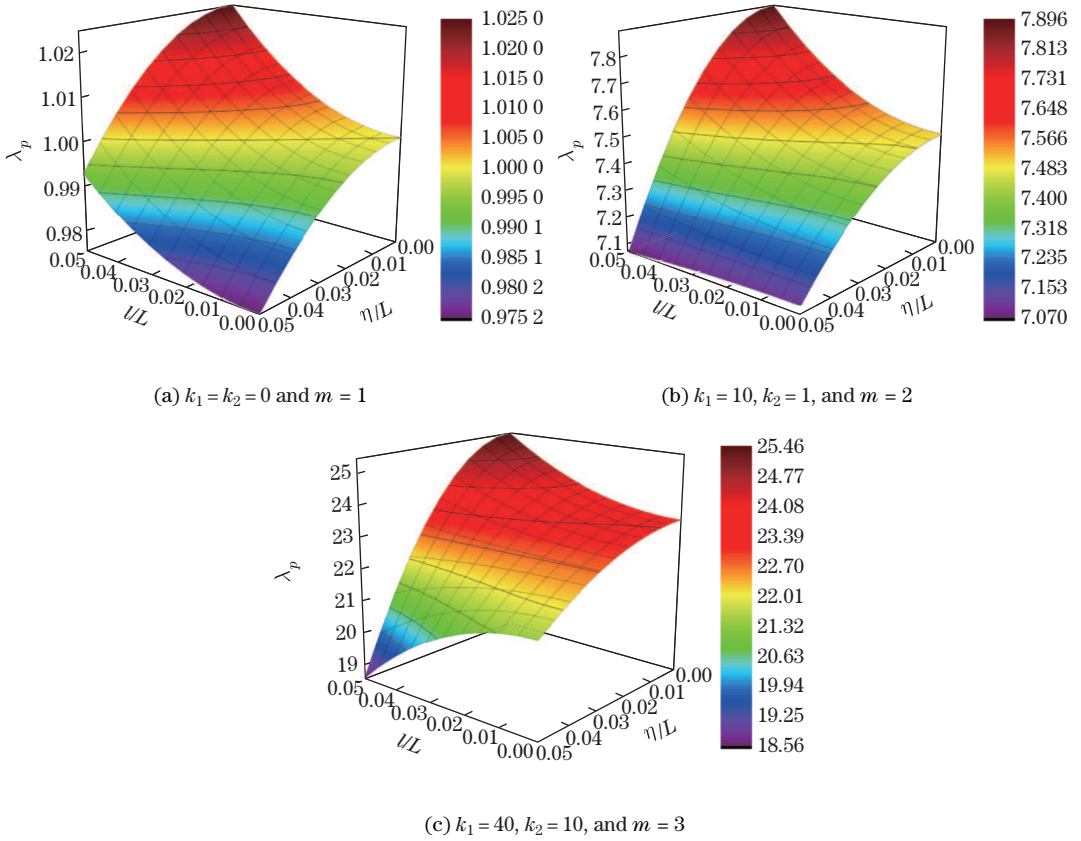

(a) $k_1 = k_2 = 0$ and $m = 1$

(b) $k_1 = 10$, $k_2 = 1$, and $m = 2$

(c) $k_1 = 40$, $k_2 = 10$, and $m = 3$

Fig. 9 Critical buckling loads of nanobeam with two different types of small scale parameters when $w_{\mathrm{m}} = 0$ (color online)

Figure 11 displays the size effects on the postbuckling configurations of nanobeams under different elastic foundation parameters. It can be seen that the buckling mode will jump as the elastic foundation parameters increase to some certain values, and the size effects are more sensitive to the lower-order buckling mode than the higher-order one. The reason for this is that the two small scale parameters and foundation parameters are the influencing factors on the bending rigidity of nanobeams, in which the nonlocal parameter has a tendency to reduce bending rigidity while the other two are just on the contrary. The increase in any one of the three parameters will weaken the stiffness-hardening or stiffness-softing effects caused by the other two. Consequently, the effects of strain gradient and nonlocal parameters on the postbuckling behavior decrease as the elastic foundation parameters increase. For the second-order and third-order buckling modes, their postbuckling configurations almost coincide with each other. This illustrates that whether or not we consider the small scale effects, there is only a minimal impact on nanobeams.

Figure 12 depicts the variation of postbuckling configuration of nanobeams with the maximum deflection. Three different sets of elastic foundation parameters (k_1, k_2) are considered here, i.e., (0, 0) for the buckling mode $m = 1$, (10, 1) for the buckling mode $m = 2$, and (50, 1) for the buckling mode $m = 3$. From this figure, it can be observed that the right end of nanobeams produces remarkable horizontal displacement as the axial compression increases, and therefore the postbuckling configurations of nanobeams undergo a distinct change. This result confirms that the postbuckling equilibrium paths are virtually stable for nanobeams resting on elastic foundations.

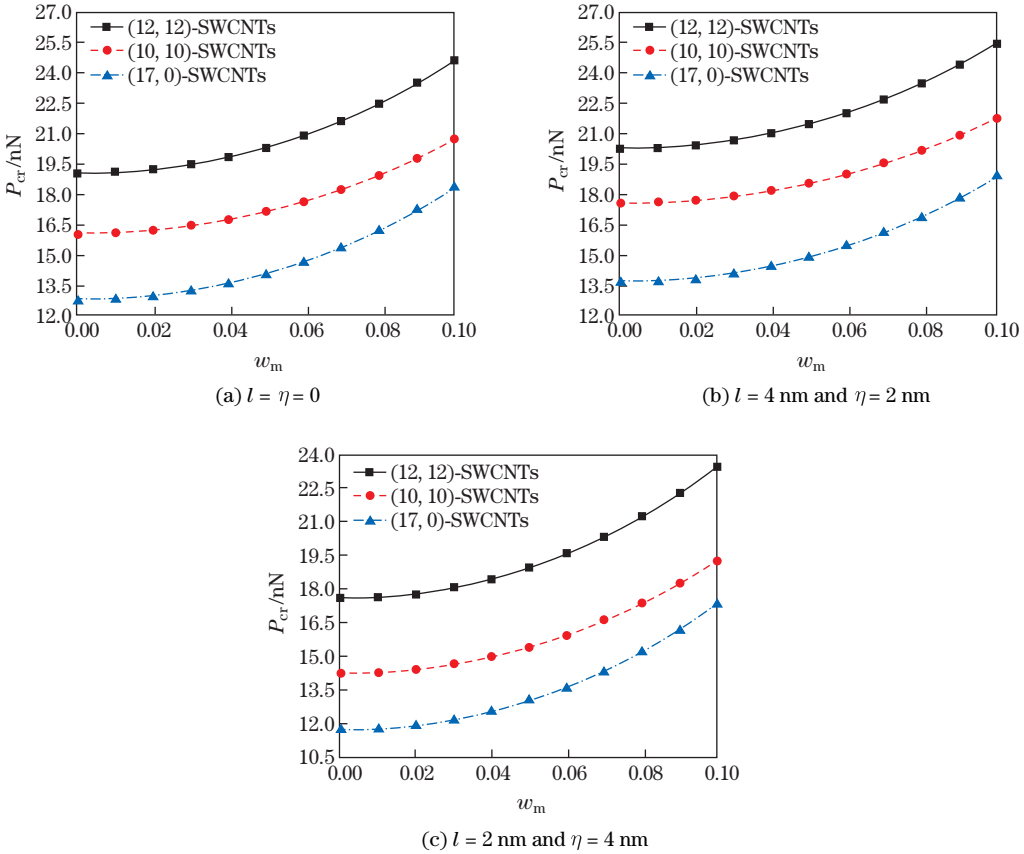

(a) $l = \eta = 0$ (b) $l = 4$ nm and $\eta = 2$ nm

(c) $l = 2$ nm and $\eta = 4$ nm

Fig. 10 Influence of two small scale parameters on postbucking behavior of SWCNTs at room temperature for $m = 3$ and $T = 300$ K

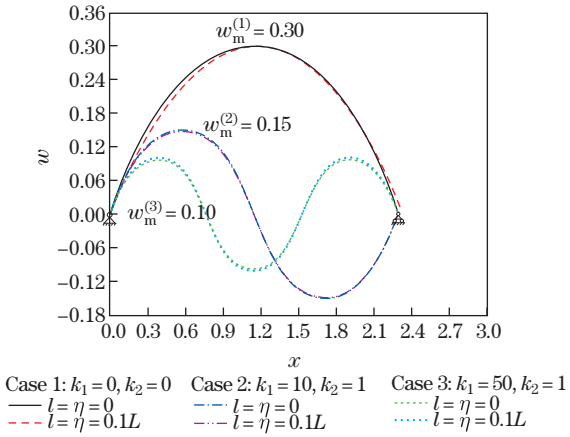

Fig. 11 Postbuckling configuration of simply supported nanobeam under different material and elastic foundation parameters (color online)

6.4 Nonlinear bending

Figure 13 investigates the influence of two kinds of small scale parameters on the nonlinear bending behavior of SWCNTs. As expected, the static deflections of SWCNTs nonlinearly increase with the increase in the nonlocal parameter or the decrease in the strain gradient parameter, and abnormal phenomenon in load-deflection curves is demonstrated when the nonlocal

parameter has a sufficiently large value, i.e., the positive static load causes negative deflection. To avoid this abnormal phenomenon, the range of values of nonlocal parameter must be restricted reasonably. The CNTs without foundation exhibit more obvious nonlinear characteristics than the CNTs with foundation. Furthermore, the (17, 0)-CNT is more likely to be deflected, the (10, 10)-CNT does less, and the (12, 12)-CNT does least.

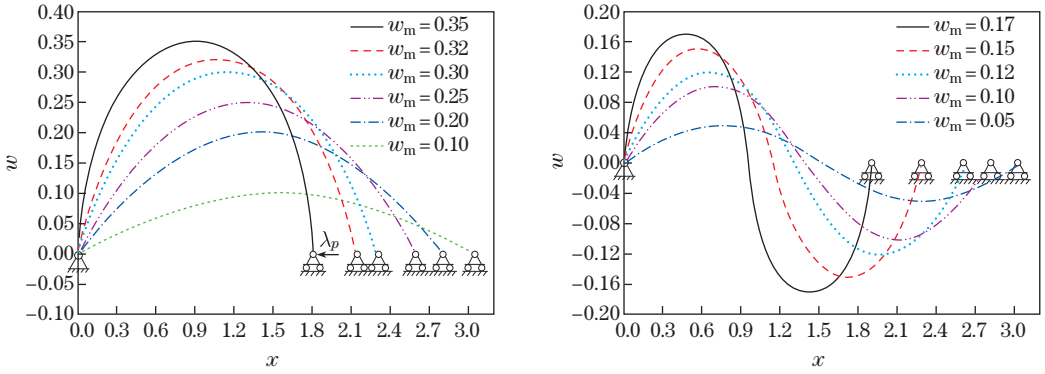

(a) $k_1 = k_2 = 0$ and $m = 1$ (b) $k_1 = 10$, $k_2 = 1$, and $m = 2$

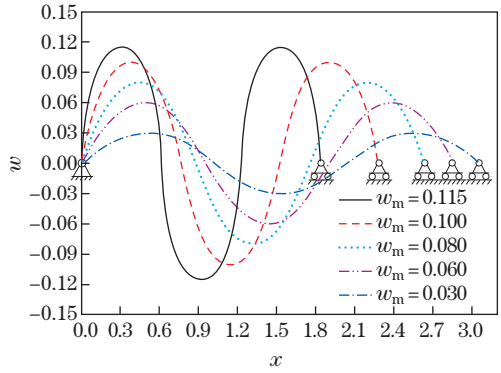

(c) $k_1 = 50$, $k_2 = 1$, and $m = 3$

Fig. 12 Variation of postbuckling configuration of simply supported nanobeam with maximum deflection under different orders of buckling modes for $l = \eta = 0$ (color online)

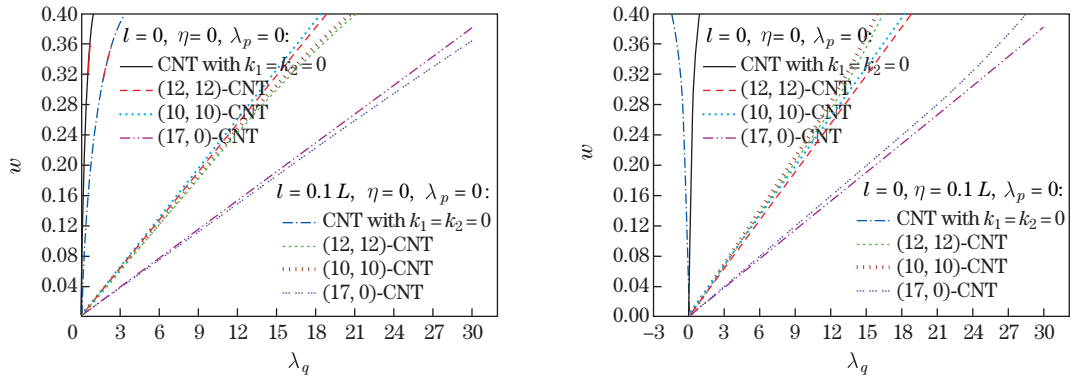

(a) $\eta = 0$ and $\lambda_p = 0$ (b) $l = 0$ and $\lambda_p = 0$

Fig. 13 Influence of nonlocal and strain gradient parameters on nonlinear bending behavior of SWCNTs (color online)

Figure 14 presents the static load-deflection curves for (12, 12)-CNTs with or without elastic foundation under two kinds of end conditions. Obviously, CNTs with movable end condition have larger deflections than the immovable case since the former is subject to less constraint. In addition, there is an excellent linear relationship between the maximum deflection and the applied transverse static load for the movable model when the elastomeric substrate is considered, while nonlinearity of the other model is still remarkable. It can be explained that the proportion of nonlinear stiffness in the total bending rigidity of movable model decreases with the increase in the elastic foundation stiffness.

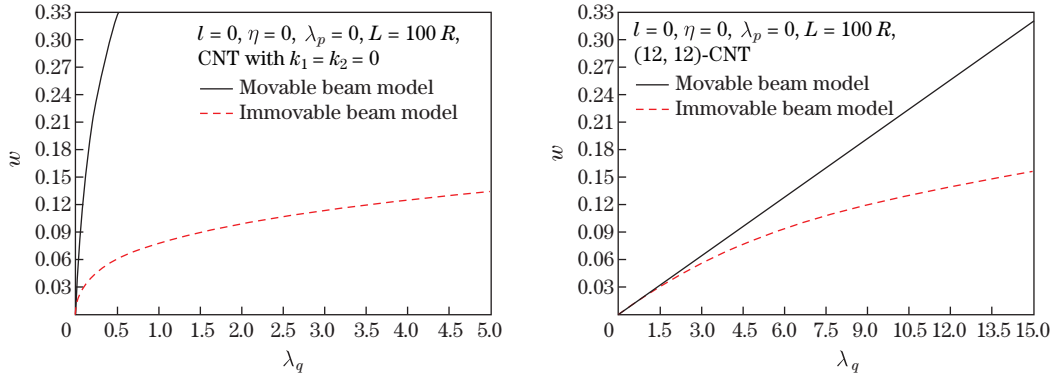

(a) Without elastic foundation (b) With elastic foundation

Fig. 14 Influence of end conditions on nonlinear bending behavior of SWCNTs (color online)

Figure 15 displays the nonlinear bending configurations of (12, 12)-SWCNTs for different amplitudes of distributed loads. As illustrated in this figure, the horizontal displacements of the movable end increase nonlinearly with the applied loads, and in the meantime, the bending configurations undergo pronounced changes. For the immovable model, however, the end displacements are always zero, and the applied static load has effect on the maximum deflection only. Besides, a similar trend can be observed that the immovable model has far less deflection than the movable model under the same transverse static loading.

Figure 16 evaluates the effect of the axial compression on the nonlinear bending configurations of (12, 12)-SWCNTs. It is clearly seen that the increase in the axial compression causes an increase in the deflection of CNTs because the bending rigidity is weakened during the loading process. Similar in the case of postbuckling, remarkable support-moving may be induced by the axial compression.

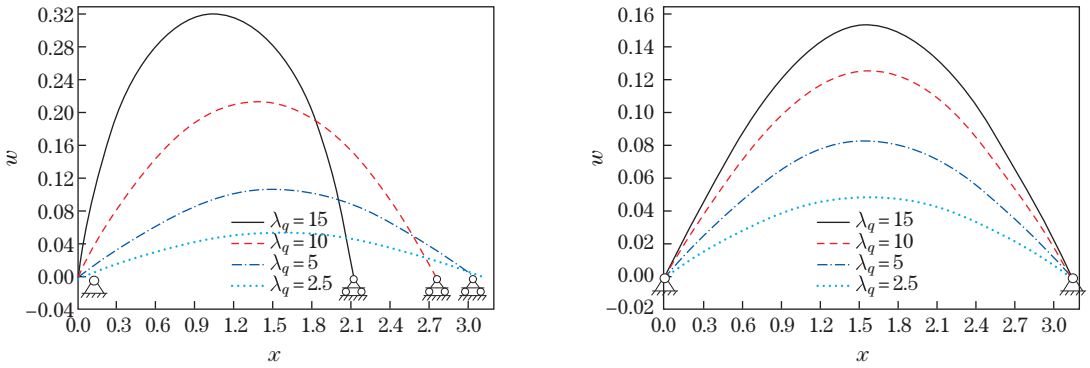

Fig. 15 Variations of nonlinear bending configurations of SWCNTs with applied transverse loads when $l = 0, \eta = 0, \lambda_p = 0$, and $L = 100R$ for (12, 12)-CNT (color online)

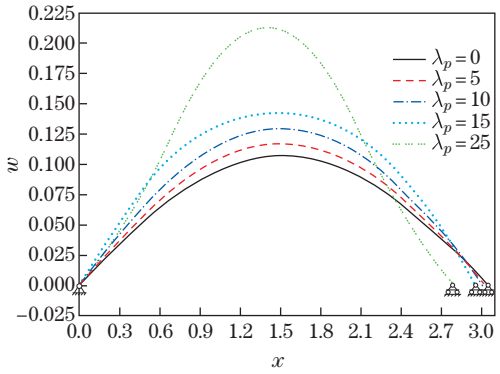

Fig. 16 Variations of nonlinear bending configurations of SWCNTs with axial compression loads when $l = 0, \eta = 0, \lambda_q = 5$, and $L = 100R$ for (12, 12)-CNT (color online)

7 Concluding remarks

Taking two kinds of size effects appearing in nanomaterials as background, we perform multi-scale nonlinear modeling and two-step perturbation analysis for large deflected nanobeams resting on an elastic foundation with movable and immovable ends. The Euler-Bernoulli beam theory with exact bending curvature and microstructural-dependency in the framework of nonlocal strain gradient elastic theory is adopted to formulate the nonlinear governing equations. The load-deflection relationship and postbuckling equilibrium path are analytically determined by a two-step perturbation method. Convergence and comparison studies are conducted to establish the accuracy of perturbation solutions. Extensive numerical examples are presented to investigate the influence of geometrical, foundation, and material parameters together with the axial compression on the nonlinear behaviors of nanobeams. The general observations can be summarized as follows. The two-step perturbation technique has a good convergence and precision as long as the value of maximum deflection is in a reasonable range. By increasing the strain gradient and foundation parameters or decreasing the nonlocal parameter, the postbuckling resistance of small scale structures is enhanced. The postbuckling equilibrium path may be more affected by the nonlocal parameter than the strain gradient parameter under the same value. The buckling mode will jump at some prescribed values of the Winkler foundation parameter. The increase in the foundation stiffnesses weakens the results from the nonlocal and strain gradient parameters. The end condition and axial tension play an important role in the nonlinear mechanical behaviors of nanobeams when the deflection tends to be large, but the two factors can be neglectable when the value of deflection is sufficiently small. The stiffness-hardening or stiffness-softing effects become increasingly important as the dimensionless thickness decreases and can be negligible as the dimensionless thickness is sufficiently large.

References

[1] RAFII-TABAR, H., GHAVANLOO, E., and FAZELZADEH, S. A. Nonlocal continuum-based modeling of mechanical characteristics of nanoscopic structures. *Physics Reports*, **638**, 1–97 (2016)

[2] LIM, C. W., ZHANG, G., and REDDY, J. N. A higher-order nonlocal elasticity and strain gradient theory and its applications in wave propagation. *Journal of the Mechanics and Physics of Solids*, **78**, 298–313 (2015)

[3] IMBODEN, M. and MOHANTY, P. Dissipation in nanoelectromechanical systems. *Physics Reports*, **534**, 89–146 (2014)

[4] ARASH, B. and WANG, Q. A review on the application of nonlocal elastic models in modeling of carbon nanotubes and graphenes. *Modeling of Carbon Nanotubes, Graphene and Their Composites*, Springer, Berlin, 57–82 (2014)

[5] ELTAHER, M. A., KHATER, M. E., and EMAM, S. A. A review on nonlocal elastic models for bending, buckling, vibrations, and wave propagation of nanoscale beams. *Applied Mathematical Modelling*, **40**, 4109–4128 (2016)

[6] WANG, K., WANG, B., and KITAMURA, T. A review on the application of modified continuum models in modeling and simulation of nanostructures. *Acta Mechanica Sinica*, **32**, 83–100 (2016)

[7] CORDERO, N. M., FOREST, S., and BUSSO, E. P. Second strain gradient elasticity of nano-objects. *Journal of the Mechanics and Physics of Solids*, **97**, 92–124 (2016)

[8] KRISHNAN, A., DUJARDIN, E., EBBESEN, T., YIANILOS, P., and TREACY, M. Young's modulus of single-walled nanotubes. *Physical Review B*, **58**, 14013 (1998)

[9] WANG, L., ZHENG, Q., LIU, J. Z., and JIANG, Q. Size dependence of the thin-shell model for carbon nanotubes. *Physical Review Letters*, **95**, 105501 (2005)

[10] DIAO, J., GALL, K., and DUNN, M. L. Atomistic simulation of the structure and elastic properties of gold nanowires. *Journal of the Mechanics and Physics of Solids*, **52**, 1935–1962 (2004)

[11] LI, C. and CHOU, T. W. A structural mechanics approach for the analysis of carbon nanotubes. *International Journal of Solids and Structures*, **40**, 2487–2499 (2003)

[12] LAM, D. C. C., YANG, F., CHONG, A. C. M., WANG, J., and TONG, P. Experiments and theory in strain gradient elasticity. *Journal of the Mechanics and Physics of Solids*, **51**, 1477–1508 (2003)

[13] LEI, J., HE, Y., GUO, S., LI, Z., and LIU, D. Size-dependent vibration of nickel cantilever microbeams: experiment and gradient elasticity. *AIP Advances*, **6**, 105202 (2016)

[14] TREACY, M. J., EBBESEN, T., and GIBSON, J. Exceptionally high Young's modulus observed for individual carbon nanotubes. *nature*, **381**, 678–680 (1996)

[15] AGRAWAL, R., PENG, B., GDOUTOS, E. E., and ESPINOSA, H. D. Elasticity size effects in ZnO nanowires — a combined experimental-computational approach. *Nano Letters*, **8**, 3668–3674 (2008)

[16] NATSUKI, T., TANTRAKARN, K., and ENDO, M. Effects of carbon nanotube structures on mechanical properties. *Applied Physics A*: *Materials Science and Processing*, **79**, 117–124 (2004)

[17] TANG, C. and ALICI, G. Evaluation of length-scale effects for mechanical behaviour of micro- and nanocantilevers: I, experimental determination of length-scale factors. *Journal of Physics D*: *Applied Physics*, **44**, 335501 (2011)

[18] RU, C. Q. Effective bending stiffness of carbon nanotubes. *Physical Review B*, **62**, 9973 (2000)

[19] WANG, Q. and VARADAN, V. Wave characteristics of carbon nanotubes. *International Journal of Solids and Structures*, **43**, 254–265 (2006)

[20] KULATHUNGA, D. D. T. K., ANG, K. K., and REDDY, J. N. Accurate modeling of buckling of single- and double-walled carbon nanotubes based on shell theories. *Journal of Physics*: *Condensed Matter*, **21**, 435301 (2009)

[21] ERINGEN, A. C. Nonlocal polar elastic continua. *International Journal of Engineering Science*, **10**, 1–16 (1972)

[22] ERINGEN, A. C. On differential equations of nonlocal elasticity and solutions of screw dislocation and surface waves. *Journal of Applied Physics*, **54**, 4703–4710 (1983)

[23] MINDLIN, R. D. Micro-structure in linear elasticity. *Archive for Rational Mechanics and Analysis*, **16**, 51–78 (1964)

[24] MINDLIN, R. D. Second gradient of strain and surface-tension in linear elasticity. *International Journal of Solids and Structures*, **1**, 417–438 (1965)

[25] TOUPIN, R. A. Elastic materials with couple-stresses. *Archive for Rational Mechanics and Analysis*, **11**, 385–414 (1962)

[26] MINDLIN, R. D. and TIERSTEN, H. F. Effects of couple-stresses in linear elasticity. *Archive for Rational Mechanics and Analysis*, **11**, 415–448 (1962)

[27] ZHOU, S., LI, A., and WANG, B. A reformulation of constitutive relations in the strain gradient elasticity theory for isotropic materials. *International Journal of Solids and Structures*, **80**, 28–37 (2016)

[28] YANG, F., CHONG, A. C. M., LAM, D. C. C., and TONG, P. Couple stress based strain gradient theory for elasticity. *International Journal of Solids and Structures*, **39**, 2731–2743 (2002)

[29] HADJESFANDIARI, A. R. and DARGUSH, G. F. Couple stress theory for solids. *International Journal of Solids and Structures*, **48**, 2496–2510 (2011)

[30] PEDDIESON, J., BUCHANAN, G. R., and MCNITT, R. P. Application of nonlocal continuum models to nanotechnology. *International Journal of Engineering Science*, **41**, 305–312 (2003)

[31] WANG, C. M., ZHANG, Y. Y., and HE, X. Q. Vibration of nonlocal Timoshenko beams. *Nanotechnology*, **18**, 105401 (2007)

[32] LIM, C. W. and WANG, C. M. Exact variational nonlocal stress modeling with asymptotic higher-order strain gradients for nanobeams. *Journal of Applied Physics*, **101**, 054312 (2007)

[33] HU, Y. G., LIEW, K. M., WANG, Q., HE, X. Q., and YAKOBSON, B. I. Nonlocal shell model for elastic wave propagation in single- and double-walled carbon nanotubes. *Journal of the Mechanics and Physics of Solids*, **56**, 3475–3485 (2008)

[34] REDDY, J. N. Nonlocal nonlinear formulations for bending of classical and shear deformation theories of beams and plates. *International Journal of Engineering Science*, **48**, 1507–1518 (2010)

[35] SHEN, H. S. and ZHANG, C. L. Nonlocal shear deformable shell model for post-buckling of axially compressed double-walled carbon nanotubes embedded in an elastic matrix. *Journal of Applied Mechanics*, **77**, 041006 (2010)

[36] SHEN, H. S. and ZHANG, C. L. Nonlocal beam model for nonlinear analysis of carbon nanotubes on elastomeric substrates. *Computational Materials Science*, **50**, 1022–1029 (2011)

[37] PENG, X. W., GUO, X. M., LIU, L., and WU, B. J. Scale effects on nonlocal buckling analysis of bilayer composite plates under non-uniform uniaxial loads. *Applied Mathematics and Mechanics* (*English Edition*), **36**(1), 1–10 (2015) https://doi.org/10.1007/s10483-015-1900-7

[38] GHORBANPOUR-ARANI, A., KOLAHDOUZAN, F., and ABDOLLAHIAN, M. Nonlocal buckling of embedded magnetoelectroelastic sandwich nanoplate using refined zigzag theory. *Applied Mathematics and Mechanics* (*English Edition*), **39**(4), 529–546 (2018) https://doi.org/10.1007/s10483-018-2319-8

[39] PARK, S. K. and GAO, X. L. Bernoulli-Euler beam model based on a modified couple stress theory. *Journal of Micromechanics and Microengineering*, **16**, 2355–2359 (2006)

[40] MA, H. M., GAO, X. L., and REDDY, J. N. A microstructure-dependent Timoshenko beam model based on a modified couple stress theory. *Journal of the Mechanics and Physics of Solids*, **56**, 3379–3391 (2008)

[41] ŞIMŞEK, M. and REDDY, J. N. Bending and vibration of functionally graded microbeams using a new higher order beam theory and the modified couple stress theory. *International Journal of Engineering Science*, **64**, 37–53 (2013)

[42] REDDY, J. N. and KIM, J. A nonlinear modified couple stress-based third-order theory of functionally graded plates. *Composite Structures*, **94**, 1128–1143 (2012)

[43] KOMIJANI, M., REDDY, J. N., and ESLAMI, M. R. Nonlinear analysis of microstructure-dependent functionally graded piezoelectric material actuators. *Journal of the Mechanics and Physics of Solids*, **63**, 214–227 (2014)

[44] KONG. S., ZHOU, S., NIE, Z., and WANG, K. Static and dynamic analysis of micro beams based on strain gradient elasticity theory. *International Journal of Engineering Science*, **47**, 487–498 (2009)

[45] WANG, B., ZHAO, J., and ZHOU, S. A micro scale Timoshenko beam model based on strain gradient elasticity theory. *European Journal of Mechanics-A/Solids*, **29**, 591–599 (2010)

[46] WANG, B., DENG, Z. C., and ZHANG, K. Nonlinear vibration of embedded single-walled carbon nanotube with geometrical imperfection under harmonic load based on nonlocal Timoshenko beam theory. *Applied Mathematics and Mechanics* (*English Edition*), **34**(3), 269–280 (2013) https://doi.org/10.1007/s10483-013-1669-8

[47] MOHAMMADIMEHR, M., FARAHI, M. J., and ALIMIRZAEI, S. Vibration and wave propagation analysis of twisted micro-beam using strain gradient theory. *Applied Mathematics and Mechanics* (*English Edition*), **37**(10), 1375–1392 (2016) https://doi.org/10.1007/s10483-016-2138-9

[48] ZHANG, B., HE, Y., LIU, D., GAN, Z., and SHEN, L. Size-dependent functionally graded beam model based on an improved third-order shear deformation theory. *European Journal of Mechanics-A/Solids*, **47**, 211–230 (2014)

[49] LI, L. and HU, Y. Buckling analysis of size-dependent nonlinear beams based on a nonlocal strain gradient theory. *International Journal of Engineering Science*, **97**, 84–94 (2015)

[50] LI, L. and HU, Y. Post-buckling analysis of functionally graded nanobeams incorporating nonlocal stress and microstructure-dependent strain gradient effects. *International Journal of Mechanical Sciences*, **120**, 159–170 (2017)

[51] LI, X., LI, L., HU, Y., DING, Z. C., and DENG, W. Bending, buckling and vibration of axially functionally graded beams based on nonlocal strain gradient theory. *Composite Structures*, **165**, 250–265 (2017)

[52] LI, L. and HU, Y. Nonlinear bending and free vibration analyses of nonlocal strain gradient beams made of functionally graded material. *International Journal of Engineering Science*, **107**, 77–97 (2016)

[53] LI, L., LI, X., and HU, Y. Free vibration analysis of nonlocal strain gradient beams made of functionally graded material. *International Journal of Engineering Science*, **102**, 77–92 (2016)

[54] LI, L., HU, Y., and LING, L. Flexural wave propagation in small-scaled functionally graded beams via a nonlocal strain gradient theory. *Composite Structures*, **133**, 1079–1092 (2015)

[55] SAHMANI, S. and FATTAHI, A. M. Small scale effects on buckling and postbuckling behaviors of axially loaded FGM nanoshells based on nonlocal strain gradient elasticity theory. *Applied Mathematics and Mechanics* (*English Edition*), **39**(4), 561–580 (2018) https://doi.org/10.1007/s10483-018-2321-8

[56] LU, L., GUO, X., and ZHAO, J. Size-dependent vibration analysis of nanobeams based on the nonlocal strain gradient theory. *International Journal of Engineering Science*, **116**, 12–24 (2017)

[57] LU, L., GUO, X., and ZHAO, J. A unified nonlocal strain gradient model for nanobeams and the importance of higher order terms. *International Journal of Engineering Science*, **119**, 265–277 (2017)

[58] LU, L., GUO, X., and ZHAO, J. On the mechanics of Kirchhoff and Mindlin plates incorporating surface energy. *International Journal of Engineering Science*, **124**, 24–40 (2018)

[59] SHEN, H. S. A novel technique for nonlinear analysis of beams on two-parameter elastic foundations. *International Journal of Structural Stability and Dynamics*, **11**, 999–1014 (2011)

[60] LI, Z. M. and QIAO, P. On an exact bending curvature model for nonlinear free vibration analysis shear deformable anisotropic laminated beams. *Composite Structures*, **108**, 243–258 (2014)

[61] WICKERT, J. Non-linear vibration of a traveling tensioned beam. *International Journal of Nonlinear Mechanics*, **27**, 503–517 (1992)

[62] SHEN, H. S. and ZHANG, J. W. Perturbation analyses for the postbuckling of simply supported rectangular plates under uniaxial compression. *Applied Mathematics and Mechanics* (*English Edition*), **9**(8), 793–804 (1988) https://doi.org/10.1007/BF02465403

[63] SHEN, H. S., XIANG, Y., and LIN, F. Nonlinear vibration of functionally graded graphene-reinforced composite laminated plates in thermal environments. *Computer Methods in Applied Mechanics and Engineering*, **319**, 175–193 (2017)

[64] SHEN, H. S., LIN, F., and XIANG, Y. Nonlinear bending and thermal postbuckling of functionally graded graphene-reinforced composite laminated beams resting on elastic foundations. *Engineering Structures*, **140**, 89–97 (2017)

[65] SHEN, H. S., HE, X. Q., and YANG, D. Q. Vibration of thermally postbuckled carbon nanotube-reinforced composite beams resting on elastic foundations. *International Journal of Non-Linear Mechanics*, **91**, 69–75 (2017)

[66] KIEN, D. K. Postbuckling behavior of beams on two-parameter elastic foundation. *International Journal of Structural Stability and Dynamics*, **4**, 21–43 (2004)

[67] NAIDU, N. R. and RAO, G. V. Stability behaviour of uniform columns on a class of two parameter elastic foundation. *Computers and Structures*, **57**, 551–553 (1995)

[68] TIMOSHENKO, S. P. and GERE, J. M. *Theory of Elastic Stability*, McGraw-Hill Book Company, New York (1961)

[69] HORIBE, T. and ASANO, N. Large deflection analysis of beams on two-parameter elastic foundation using the boundary integral equation method. *JSME International Journal Series A Solid Mechanics and Material Engineering*, **44**, 231–236 (2011)

Appendix A

$$\lambda_0 = m^2 + \frac{k_1}{m^2} + k_2 + m^4\pi^2(d_5 - m^2\pi^2 d_4),$$

$$\gamma_{33} = f_{33}/(729\pi^2 m^6(9\pi^2 m^2 d_4 - d_5) - (81m^4 + 9m^2 k_2 - 9m^2\lambda_0 + k_1)),$$

$$\gamma_{53} = f_{53}/(729\pi^2 m^6(9\pi^2 m^2 d_4 - d_5) - (k_1 + 9m^2 k_2 + 81m^4 - 9\lambda_0 m^2)),$$

$$\gamma_{55} = f_{55}/(15\ 625\pi^2 m^6(25\pi^2 m^2 d_4 - d_5) - (k_1 + 25m^2 k_2 + 625m^4 - 25\lambda_0 m^2)),$$

$$\gamma_{73} = f_{73}/(729\pi^2 m^6(9\pi^2 m^2 d_4 - d_5) - (k_1 + 9m^2 k_2 + 81m^4 - 9\lambda_0 m^2)),$$

$$\gamma_{75} = f_{75}/(15\ 625\pi^2 m^6(25\pi^2 m^2 d_4 - d_5) - (k_1 + 25m^2 k_2 + 625m^4 - 25\lambda_0 m^2)),$$

$$\gamma_{77} = f_{77}/(117\ 649\pi^2 m^6(81\pi^2 m^2 d_4 - d_5) - (k_1 + 49m^2 k_2 + 2\ 401m^4 - 49\lambda_0 m^2)).$$

$$f_{31} = -\frac{1}{8}\pi^2 m^4(4m^4\pi^2(m^2\pi^2 d_4 - d_5) + 3\lambda_0 - 4m^2),$$

$$f_{33} = -\frac{3}{8}\pi^2 m^4(4m^4\pi^2(61m^2\pi^2 d_4 - 7d_5) + \lambda_0 - 4m^2),$$

$$\begin{aligned} f_{51} = &-\frac{9}{8}\pi^2 m^4\gamma_{33}(4m^4\pi^2(61m^2\pi^2 d_4 - 7d_5) + \lambda_0 - 4m^2) \\ &- \frac{3}{64}\pi^2 m^2(8\pi^4 m^8(11\pi^2 m^2 d_4 - 2d_5) + \pi^2 m^4(5\lambda_0 - 8m^2) + 8f_{31}), \end{aligned}$$

$$\begin{aligned} f_{53} = &-\frac{9\gamma_{33}}{4}(4\pi^4 m^8(365\pi^2 m^2 d_4 - 41d_5) + \pi^2 m^4(3\lambda_0 - 20m^2) + 4f_{31}) \\ &- \frac{3\pi^2 m^2}{128}(8\pi^4 m^8(397\pi^2 m^2 d_4 - 46d_5) + \pi^2 m^4(15\lambda_0 - 56m^2) + 16f_{31}), \end{aligned}$$

$$\begin{aligned} f_{55} = &-\frac{45}{8}\pi^2 m^4\gamma_{33}(4m^4\pi^2(1\ 363m^2\pi^2 d_4 - 59d_5) + \lambda_0 - 12m^2) \\ &- \frac{15}{128}\pi^4 m^6(8m^4\pi^2(411m^2\pi^2 d_4 - 16d_5) + \lambda_0 - 8m^2), \end{aligned}$$

$$\begin{aligned} f_{71} = &-\frac{9}{4}\pi^2 m^4\gamma_{33}^2(4m^4\pi^2(365m^2\pi^2 d_4 - 41d_5) + 3\lambda_0 - 20m^2) \\ &- \frac{3\pi^2 m^2}{128}(40\pi^4 m^8(397m^2\pi^2 d_4 - 46d_5) + 5\pi^2 m^4(15\lambda_0 - 56m^2) + 48f_{31})\gamma_{33} \\ &- \frac{\pi^2 m^2}{1\ 024}(64\pi^6 m^{10}(95\pi^2 m^2 d_4 - 14d_5) + 5\pi^4 m^6(35\lambda_0 - 64m^2) + 16(15f_{31}\pi^2 m^2 + 24f_{51})) \\ &- \frac{9}{8}\pi^2 m^4\gamma_{53}(4m^4\pi^2(61\pi^2 m^2 d_4 - 7d_5) + \lambda_0 - 4m^2), \end{aligned}$$

$$\begin{aligned} f_{73} = &-\frac{9\gamma_{33}}{64}(24\pi^6 m^{10}(1\ 321\pi^2 m^2 d_4 - 102d_5) + 3\pi^4 m^6(15\lambda_0 - 88m^2) + 16(3f_{31}\pi^2 m^2 + 4f_{51})) \\ &- \frac{9\gamma_{53}}{4}(4\pi^4 m^8(365\pi^2 m^2 d_4 - 41d_5) + \pi^2 m^4(3\lambda_0 - 20m^2) + 4f_{31}) \\ &- \frac{45}{8}\pi^2 m^4\gamma_{55}(4m^4\pi^2(1\ 363m^2\pi^2 d_4 - 59d_5) + \lambda_0 - 12m^2) \\ &- \frac{3\pi^2 m^2}{1\ 024}(384\pi^6 m^{10}(76\pi^2 m^2 d_4 - 7d_5) + 3\pi^4 m^6(35\lambda_0 - 128m^2) + 8(15f_{31}\pi^2 m^2 + 16f_{51})), \end{aligned}$$

$$
\begin{aligned}
f_{75} =& -\frac{45\pi^2 m^4}{8}(\,4m^4\pi^2(4\ 271m^6 d_4\pi^4 - 197d_5) + 3\,\lambda_0 - 44\,m^2)\gamma_{33}^2 \\
&- \frac{15\pi^2 m^2}{32}(8\pi^4 m^8(8\ 209\pi^2 m^2 d_4 - 358d_5) + \pi^2 m^4(15\,\lambda_0 - 152\,m^2) + +12 f_{31})\gamma_{33} \\
&- \frac{45\,\pi^2 m^4}{8}(4m^4\pi^2(1\ 363m^2\pi^2 d_4 - 59d_5) + \lambda_0 - 12\,m^2)\gamma_{53} \\
&- \frac{25}{4}(4\pi^4 m^8(7\ 813\,\pi^2 m^2 d_4 - 313d_5) + \pi^2 m^4(3\,\lambda_0 - 52m^2) + 4\,f_{31})\gamma_{55} \\
&- \frac{5\pi^4 m^4}{1\ 024}(128\pi^4 m^8(797\,\pi^2 m^2 d_4 - 35d_5) + \pi^2 m^4(35\,\lambda_0 - 256\,m^2) + 24 f_{31}), \\
f_{77} =& -\frac{63}{8}\pi^2 m^4\gamma_{33}^2(4m^4\pi^2(29\ 777m^2\pi^2 d_4 - 641d_5) + 3\,\lambda_0 - 68m^2) \\
&- \frac{21}{128}\,m^6\pi^4\gamma_{33}(8\,m^4\pi^2(48\ 421m^2\pi^2 d_4 - 1\ 102d_5) + 15\,\lambda_0 - 248\,m^2) \\
&- \frac{35}{8}\pi^2 m^4\gamma_{55}(4m^4\pi^2(33\ 319\,m^2\pi^2 d_4 - 757d_5) + 3\,\lambda_0 - 76m^2) \\
&- \frac{7\pi^6 m^8}{1\ 024}(\,64m^4\pi^2(1\ 471m^2\pi^2 d_4 - 34d_5) + 5\,\lambda_0 - 64\,m^2).
\end{aligned}
$$

Appendix B

The relationship between the uniformly distributed transverse load and the maximum deflection can be written as

$$
\begin{aligned}
\lambda_q =& -\frac{1}{4}m\pi(\pi^2 m^6(d_4\pi^2 m^2 - d_5) - (k_1 + m^2 k_2 + m^4))w_{\mathrm{m}} \\
&- \frac{1}{4}m\pi(m^6\pi^2\gamma_{33}(m^2\pi^2 d_4 - d_5) - \gamma_{33}(k_1 + m^2 k_2 + m^4) - f_{31})w_{\mathrm{m}}^3,
\end{aligned}
$$

in which

$$
\begin{aligned}
\gamma_{33} &= \frac{f_{33}}{729\pi^2 m^6(9\pi^2 m^2 d_4 - d_5) - (k_1{+}9m^2 k_2{+}81m^4)}, \\
f_{31} &= \frac{1}{4}\,\pi^2 m^4(2\,m^4\pi^2(\,m^2\pi^2 d_4 - d_5) + d_3 - 2\,m^2), \\
f_{33} &= -\frac{3}{2}\,m^6\pi^2(m^2\pi^2(m^2\pi^2 d_4 - d_5) - 1).
\end{aligned}
$$